Inorganic Chemistry

pubs.acs.org/IC Article

Ruthenium(II) Diphosphine Complexes with Mercapto Ligands That Inhibit Topoisomerase IB and Suppress Tumor Growth In Vivo

Monize M. da Silva, Gabriel H. Ribeiro,* Mariana S. de Camargo, Antônio G. Ferreira, Leandro Ribeiro, Marília I. F. Barbosa, Victor M. Deflon, Silvia Castelli, Alessandro Desideri, Rodrigo S. Corrêa, Arthur B. Ribeiro, Heloiza D. Nicolella, Saulo D. Ozelin, Denise C. Tavares, and Alzir A. Batista*

Cite This: *Inorg. Chem.* 2021, 60, 14174−14189 Read Online

ACCESS | Metrics & More | Article Recommendations | Supporting Information

ABSTRACT: Ruthenium(II) complexes (**Ru1**−**Ru5**), with the general formula $[Ru(N\text{-}S)(dppe)_2]PF_6$, bearing two 1,2-*bis*(diphenylphosphino)-ethane (dppe) ligands and a series of mercapto ligands (N-S), have been developed. The combination of these ligands in the complexes endowed hydrophobic species with high cytotoxic activity against five cancer cell lines. For the A549 (lung) and MDA-MB-231 (breast) cancer cell lines, the IC_{50} values of the complexes were 288- to 14-fold lower when compared to cisplatin. Furthermore, the complexes were selective for the A549 and MDA-MB-231 cancer cell lines compared to the MRC-5 nontumor cell line. The multitarget character of the complexes was investigated by using *calf thymus* DNA (CT DNA), human serum albumin, and human topoisomerase IB (hTopIB). The complexes potently inhibited hTopIB. In particular, complex $[Ru(dmp)(dppe)_2]PF_6$ (**Ru3**), bearing the 4,6-diamino-2-mercaptopyrimidine (dmp) ligand, effectively inhibited hTopIB by acting on both the cleavage and religation steps of the catalytic cycle of this enzyme. Molecular docking showed that the **Ru1**−**Ru5** complexes have binding affinity by active sites on the hTopI and hTopI-DNA, mainly via π-alkyl and alkyl hydrophobic interactions, as well as through hydrogen bonds. Complex **Ru3** displayed significant antitumor activity against murine melanoma in mouse xenograph models, but this complex did not damage DNA, as revealed by Ames and micronucleus tests.

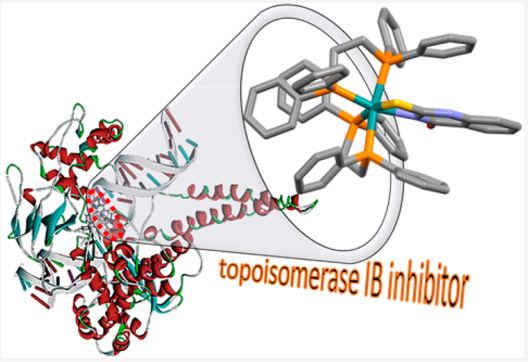

INTRODUCTION

Since the anticancer properties of the first ruthenium complexes were tested, several classes of these metal complexes that exert cytotoxic activity have been investigated both in vitro and in vivo.[1−9] The well-established synthetic chemistry of ruthenium provides numerous approaches for the development of new complexes containing this metal, and their structural diversities reflect on their anticancer properties against different types of cancer cells.[10] Cell death induced by ruthenium complexes can occur via different mechanisms of action given that these complexes can inhibit the action of various intracellular and extracellular pharmacological targets that play relevant roles in cellular processes.[11−17]

Within this theme, we had previously designed, synthesized, and studied the chemistry, reactivity, and cytotoxic properties of ruthenium(II) phosphine complexes bearing mercapto ligands (N-S).[18−21] Herein, we will focus on the cytotoxicity of these complexes and their interaction with biological molecules, mainly DNA[22,23] and proteins,[24,25] to get information about their mechanism of action and to try to shed some light on possible structure−activity relationships in these systems. Remarkably, complexes with the general formulas $[Ru(N\text{-}S)(bipy)(dppb)]PF_6$ and $[Ru(N\text{-}S)(bipy)(PPh_3)_2]PF_6$ [where bipy = 2,2′-bipyridine, dppb = 1,4-bis(diphenylphosphino)butane, and PPh_3 = triphenylphosphine] exert promising cytotoxic activity against different cancer cell lines in vitro.[19,21] The most active complexes of these series have IC_{50} values ranging from 10 to 0.05 μM, especially against the human lung (A549) and breast (MDA-MB-231) cancer cell lines. In contrast, neutral complexes with the general formula $[Ru(N\text{-}S)_2(dppb)]$ display low cytotoxicity.[23,26] The ruthenium(II) phosphine complexes exert cytotoxic effects by different mechanisms of action, which are distinct from the mechanisms of action of platinum-based drugs. For example, complex $[Ru(mtz)(bipy)(dppb)]PF_6$ (mtz = 1,3-thiazolidine-2-thione) has a broad spectrum of anticancer properties.[21,22] Detailed mechanistic studies have suggested that this complex induces apoptosis mediated by the MAPK ERK1/2 inhibitor pathway in HepG2 cells. This points to an

Received: May 27, 2021
Published: September 3, 2021

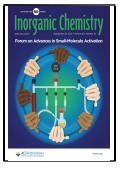

https://doi.org/10.1021/acs.inorgchem.1c01539
Inorg. Chem. 2021, 60, 14174−14189

association with a prosurvival function, causing ERK1/2 activation induced by DNA damage and leading to apoptotic cell death. Notably, this complex shows highly promising antitumor activity. The complex inhibits HepG2 cell growth in C.B-17 SCID mice more effectively than doxorubicin, a commercial anticancer drug.[22]

Ruthenium(II) phosphine complexes present an important feature described in different works: lipophilicity,[10,27,28] which is essential for their cytotoxic activity.[10] Lipophilicity is believed to be crucial for efficient cellular uptake of these complexes, as well as for their interaction with biomolecules. The biological targets and the mechanism of actions of ruthenium(II) phosphine complexes have not been fully elucidated, but there is evidence that the complexes act as multitargets, such as topoisomerase, proteassoma 26S, and DNA. Ruthenium(II) phosphine complexes containing mercapto ligands have been reported as potent inhibitors of human DNA topoisomerase IB, but extensive studies on this subject are still necessary.[24,29]

Human topoisomerase IB (hTopIB) is a key nuclear enzyme involved in the replication, transcription, recombination, and chromosome condensation of the DNA; it is highly expressed in many tumors.[30] Well-known hTopIB-targeting drugs, such as camptothecin and its derivatives, are among the most used chemotherapeutic drugs in cancer treatment.[31−34] hTopIB catalyzes DNA relaxation by transiently cleaving one strand of the DNA double helix and religating the DNA strand.[35] Mechanistically, formation of the cleaved complex is a critical event during the cell cycle because the cell is seriously compromised by poisoning of the DNA-hTopIB complex. The inhibitors that act in this process are known as "topoisomerase poisons". The inhibitors that prevent religation of one DNA strand are called catalytic inhibitors. The stalled hTopIB can directly affect progression of the cell processes, producing double DNA strand damage and consequently inducing cell death.[36,37]

Bearing these facts in mind, we described the development of new ruthenium(II) complexes bearing two 1,2-bis-(diphenylphosphino)ethane (dppe) ligands and different mercapto ligands. Here, we evaluate the cytotoxic activity of these new complexes, namely, $[Ru(mtz)(dppe)_2]PF_6$ (**Ru1**), $[Ru(mmi)(dppe)_2]PF_6$(**Ru2**), $[Ru(dmp)(dppe)_2]PF_6$ (**Ru3**), $[Ru(mpca)(dppe)_2]PF_6$ (**Ru4**), and $[Ru(2mq)(dppe)_2]PF_6$ (**Ru5**) [where mtz = 1,3-thiazolidine-2-thione, mmi = mercapto-1-methylimidazole, dmp = 4,6-diamino-2-mercapto-pyrimidine, mpca = 6-mercaptopyridine-3-carboxylic acid, and 2mq = 2-mercapto-4(3*H*)-quinazoline] against a panel of cancer cell lines and a nontumor cell line. We also assess the multitarget [e.g., toward DNA and human serum albumin (HSA)] character of these complexes. Furthermore, we investigate the ability of these complexes to inhibit hTopIB during relaxation of supercoiled DNA. Moreover, we investigate whether complex **Ru3** disrupts the cleavage and religation steps of the hTopIB catalytic cycle. Finally, we evaluate the mutagenicity of complex **Ru3** and the effects of this complex on melanoma tumor growth in vivo in mouse xenograph models.

RESULTS AND DISCUSSION

Characterization of the Complexes. Complexes **Ru1**−**Ru5** (Figure 1) were prepared by reacting the precursor *cis*-$[RuCl_2(dppe)_2]$ with appropriate equivalents of the corresponding mercapto ligand in methanol/dichloromethane

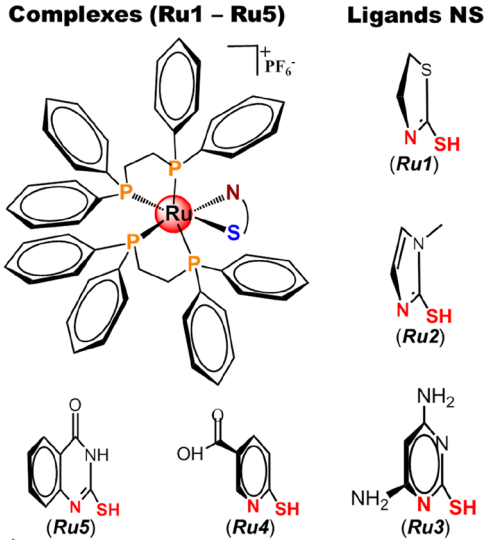

Figure 1. General chemical structures of complexes **Ru1**−**Ru5**.

under an argon atmosphere and reflux for 12 h. The complexes **Ru1**−**Ru5** in good yields (82−95%), as yellow solids, were isolated and characterized by the usual techniques. The structures of complexes **Ru1**−**Ru5** and their purities were confirmed in solution and the solid state.

The single-crystal X-ray structures of complexes **Ru1** (CCDC 2079011), **Ru2** (CCDC 2079012), **Ru4** (CCDC 2079013), and **Ru5** (CCDC 2079014) (Figure 2) were determined. Tables S3 and S4 list the selected bond distances and bond angles. All of the complexes were in the six-coordination mode, consistent with a distorted octahedral geometry around the Ru^{II} center, which was coordinated with two dppe ligands and one mercapto ligand.

The mercapto ligands were coordinated to the metal center in a bidentate manner, through S and N atoms, with the N1 atom trans to the P3 atom and, the S1 atom trans to the P2 atom. The P1 and P4 atoms occupied positions in the equatorial plane and were situated trans to each other. Compared to the Ru−P bond distances (Table S1), the bond lengths involving the axial P atoms (P1 and P4) were slightly longer than those involving the equatorial P atoms (P2 and P3), which could be related to a competitive effect due to the trans influence between the P atoms, causing the Ru−P bond to elongate along the axial position. The geometric parameters (bond lengths, bond angles, and torsional angles) obtained for complexes **Ru1**−**Ru5** were consistent with the expected values for related ruthenium(II) complexes bearing N,S-donor ligands.[20,38]

In the region 3200−3100 cm^{-1} of the IR spectra of complexes **Ru1**−**Ru5**, the absence of a broad band confirms the monoanionic coordination of the mercapto ligands to ruthenium. The spectra of the free mercapto ligands are characterized by the presence of a broad band referring to the ν(N−H) mode. Characteristic vibrations assigned to the ν(C−S) and δ(C−S) modes occur in the range 1225−1275 cm^{-1} (Figures S1−S5).[6,11,14,19]

The resolved patterns of resonances in the ^1H and ^{13}C $\{^1H\}$ NMR spectra are consistent with low symmetry of the ruthenium(II) complexes (Figures S6−S31). For all of the ruthenium(II) complexes, the $^{31}P\{^1H\}$ NMR spectra presented four distinct signals of double double doublets (ddd), consistent with ABMX pattern spin systems. Thus, the four

https://doi.org/10.1021/acs.inorgchem.1c01539
Inorg. Chem. 2021, 60, 14174−14189

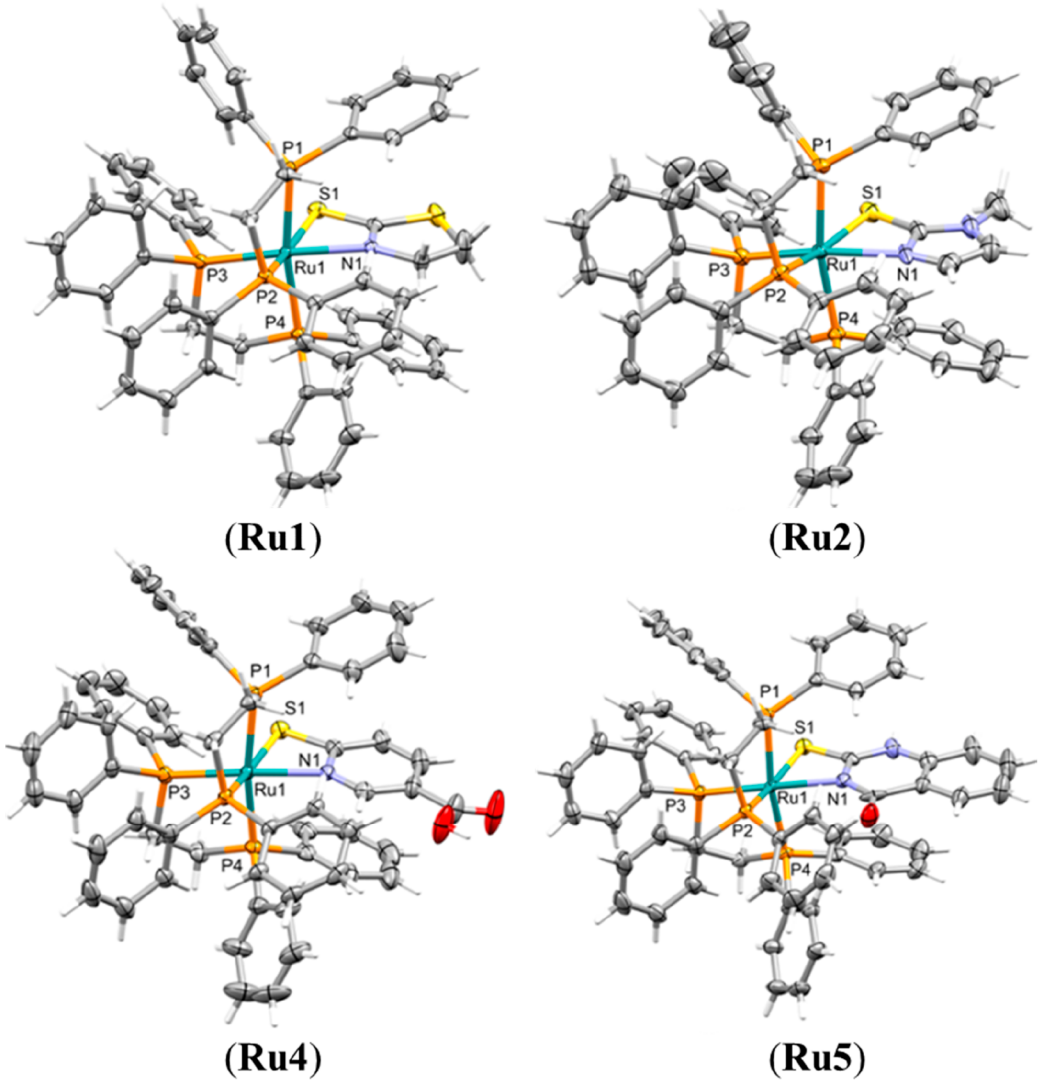

Figure 2. ORTEP view of the ruthenium(II) complexes showing the atom labels and 50% probability ellipsoids. All H atoms and anions have been omitted for clarity.

Table 1. IC_{50} Values[a] (μmol L^{-1}) of the In Vitro Cytotoxic Activity of Complexes Ru1−Ru5, Precursor *cis*-[$RuCl_2(dppe)_2$], and Cisplatin (Reference Drug) against the MCF-7, MDA-MB-231, A549, DU-145, and HepG2 Cancer Cell Lines and the MRC-5 Nontumor Human Lung Cell Line

	IC_{50} (μM)					
complex	A549	MDA-MB-231	MCF-7	DU-145	HepG2	MRC-5
Ru1	0.07 ± 0.03	0.03 ± 0.01	3.68 ± 0.89	0.35 ± 0.12	1.94 ± 0.06	0.79 ± 0.10
Ru2	0.12 ± 0.07	0.08 ± 0.02	5.24 ± 0.08	1.46 ± 0.05	5.80 ± 0.70	0.81 ± 0.12
Ru3	0.89 ± 0.09	0.20 ± 0.02	8.14 ± 0.45	3.90 ± 0.99	5.95 ± 0.09	2.62 ± 0.42
Ru4	1.02 ± 0.09	1.97 ± 0.03	9.01 ± 1.53	5.92 ± 0.75	25.45 ± 0.68	19.59 ± 0.51
Ru5	0.05 ± 0.01	0.30 ± 0.03	6.27 ± 0.25	6.02 ± 0.10	7.37 ± 0.72	5.72 ± 0.64
precursor	0.40 ± 0.06	0.77 ± 0.04	24.26 ± 4.08	0.61 ± 0.20	44.99 ± 0.11	2.83 ± 0.06
cisplatin	14.40 ± 1.45	2.44 ± 0.39	13.98 ± 2.02	2.33 ± 0.40	16.31 ± 0.74	29.09 ± 0.79

[a]Data are expressed as mean ± SD (n = 3) with 95% confidence intervals. [b]For the free ligands, IC_{50} > 50 μM; assay involved incubation for 48 h.

P atoms were chemically and magnetically nonequivalent in the ruthenium(II) complexes.

The UV−vis absorption spectra in solutions of CH_2Cl_2 for the complexes (Figure S32) are characterized by high-energy bands around 250 nm, which can be assigned to ligand-localized, intraligand $\pi-\pi^*$ transitions. Moreover, the complexes exhibit lower-energy bands at about 350 nm, with weak intensity, which can be assigned as metal-to-ligand charge-transfer transitions, Ru($d\pi$) to ligand (π^*). The cyclic voltammetry experiments of complexes **Ru1−Ru5**, carried out in CH_2Cl_2 solutions (Figure S33 and Table S5), presented a quasi-reversible process, corresponding to one-electron Ru^{II}/

https://doi.org/10.1021/acs.inorgchem.1c01539
Inorg. Chem. 2021, 60, 14174−14189

Table 2. SI Values of Complexes Ru1−Ru5 for Cancer Cell Lines

	SI[b]				
complex	A549	MDA-MB-231	MCF-7	DU-145	HepG2
Ru1	11 ± 5	26 ± 9	0.21 ± 0.06	2.3 ± 0.8	0.41 ± 0.05
Ru2	7 ± 4	10 ± 3	0.15 ± 0.02	0.55 ± 0.08	0.14 ± 0.03
Ru3	2.9 ± 0.6	13 ± 2	0.32 ± 0.05	0.7 ± 0.2	0.44 ± 0.07
Ru4	19 ± 2	9.9 ± 0.3	2.2 ± 0.4	3.3 ± 0.4	0.77 ± 0.03
Ru5	114 ± 26	19 ± 3	0.9 ± 0.1	0.9 ± 0.1	0.78 ± 0.12
precursor	7 ± 1	3.7 ± 0.2	0.12 ± 0.02	5 ± 1	0.06 ± 0.01
cisplatin	2.0 ± 0.2	11 ± 1	2.1 ± 0.3	12 ± 2	1.78 ± 0.09

[a]The SI of each complex was calculated using the following formula: SI = IC_{50}(MRC-5)/IC_{50}(cancer cell line). [b]Data are expressed with propagated uncertainties of the SI.

Ru^{III}, with oxidation-wave potentials, Epa (anodic peak potential), in the range 1116−1360 mV. The electrochemical behavior of these complexes, in cyclic voltammetric experiments, was similar to that found for other ruthenium compounds reported in the literature, such as the [Ru(pymS)(dppe)$_2$]PF_6 (Epa = 1.47 mV) and [Ru(pymS)(dppm)$_2$]PF_6 [pymS = 2-mercaptopyrimidine; dppm = 1,1-(diphenylphosphino)methane] complexes (Epa = 1.42 mV).[13]

Stability in Aqueous Medium. Complexes **Ru1**−**Ru5** are soluble and stable in solvents such as dimethyl sulfoxide (DMSO), *N*,*N*-dimethylformamide, and chlorinated solvents. However, the complexes are not soluble in a pure aqueous medium, but they are soluble and stable in a mixture of 1:99 DMSO/aqueous medium at micromolar concentrations, which were used for biological studies. For biological experiments, complexes **Ru1**−**Ru5** were initially dissolved in the DMSO solvent and subsequently diluted in the respective medium. Therefore, the stability of the new ruthenium(II) complexes dissolved in DMSO were evaluated by $^{31}P\{^1H\}$ NMR spectroscopy in time course of 0, 48, and 72 h (Figures S34−S38). It is worth mentioning that we evaluated the cytotoxic activity of the ruthenium(II) complexes against cells for an incubation period of 48 h. From the $^{31}P\{^1H\}$ NMR spectra, the signals of the ruthenium(II) complexes remained unchanged over 72 h, which attested to their integrity in the DMSO solvent.

Cytotoxicity Assays and Partition Coefficient (log *P*). We evaluated the cytotoxic activities (Table 1) of complexes **Ru1**−**Ru5** against five cancer cell lines, namely, A549 (human lung epithelial), MDA-MB-231 (mesenchymal-like human triple-negative breast adenocarcinoma), MCF-7 (epithelial-like estrogen-dependent human breast adenocarcinoma), DU-145 (human prostate carcinoma), and HepG2 (human hepatocellular carcinoma). To determine the selectivity index (SI; Table 2), we also assessed the cytotoxic activities of complexes **Ru1**−**Ru5** against MRC-5 nontumor human lung cell line (Table 1).

First, the precursor *cis*-[$RuCl_2$(dppe)$_2$] was active against all tested tumor lines, especially for the DU-145, A549, and MDA-MB-231 cells. The precursor bearing two dppe ligands was 36-, 3-, and 4-fold more active than cisplatin, respectively, with respect to these tumor cells. In general, replacement of the chlorido ligands in the precursor *cis*-[$RuCl_2$(dppe)$_2$] by mercapto ligands was highly advantageous: it afforded new cationic complexes containing two diphosphine ligands, leading to high cytotoxicity, and mainly most of the complexes were more cytotoxic compared to the precursor, cisplatin, and all free mercapto ligands. All of the tested ruthenium(II) complexes were more active against the A549 (lung) and MDA-MB-231 (breast) cancer cell lines than toward the other studied cancer cells. For the A549 cancer cell line, complexes **Ru1**−**Ru5** exhibited 288−14-fold lower IC_{50} values than that cisplatin. Furthermore, the IC_{50} values for the MDA-MB-231 cell line were 81−1 times lower compared to that of the commercial drug. However, it is worth mentioning that, toward A549 cells, complexes **Ru3** and **Ru4** were approximately 2.2- and 2.6-fold, respectively, less active than the precursor *cis*-[$RuCl_2$(dppe)$_2$]. Similarly, for the MDA-MB-231 cells, complex **Ru3** was less active compared to its respective precursor. Surprisingly, for the DU-147 cells, the precursor *cis*-[$RuCl_2$(dppe)$_2$] was more effective than most of the new complexes. However, for the vast majority of the cases, the addition of the mercapto ligands to the precursors forms products that are more cytotoxic against the tumor cells.

Complexes **Ru1**−**Ru5** were more cytotoxic against the A549 and MDA-MB-231 cancer cell lines compared to the MRC-5 nontumor cell line. All of the ruthenium(II) complexes, including the precursor *cis*-[$RuCl_2$(dppe)$_2$], exhibited SIs (Table 2) in the range of 3−35 regarding the pair MRC-5/MDA-MB-231. Also, SIs of the new complexes were greater than that of cisplatin for the pair MRC-5/A549. As far as we know, the SI value of **Ru5** of 114 for the pair MRC-5/A549 is the highest described for ruthenium(II) phosphine complexes.

These new results, combined with the data previously reported by our group, have provided more solid insight into ruthenium(II) phosphine complexes:

(I) These complexes exhibited remarkable cytotoxic action against the A549 and MDA-MB-231 cancer cell lines, which are better than most of the complexes reported in the literature.[39−44] This behavior probably resulted from the good lipophilicity of this class of complexes.

(II) The cytotoxic activity of the ruthenium(II) complexes was dependent on the auxiliary mercapto ligands. In general, complexes **Ru1** and **Ru2** were more cytotoxic than that complexes **Ru3**−**Ru5**. Structurally, complexes **Ru1** and **Ru2** are characterized by mercapto ligands without functional groups or "electrophilic groups" attached to the rings. Complexes **Ru3**−**Ru5** have mercapto ligands with "donor groups" in the mercapto ligand, such as amine and carbonyl moieties. This trend for mercapto ligands in ruthenium(II) complexes has been reported.[10] However, no trend concerning the selectivity of the complexes has been observed.

(III) The presence and quantity of phosphine ligands were key for the efficacy of the ruthenium(II) complexes.[28,45,46] The complexes described herein were more active than the respective analogous complexes bearing the same mercapto ligands, [Ru(N-S)(bipy)(dppb)]PF_6[21] and [Ru(N-S)$_2$(dppb)].[26] In the case of the A549 cancer cells, the

https://doi.org/10.1021/acs.inorgchem.1c01539
Inorg. Chem. 2021, 60, 14174−14189

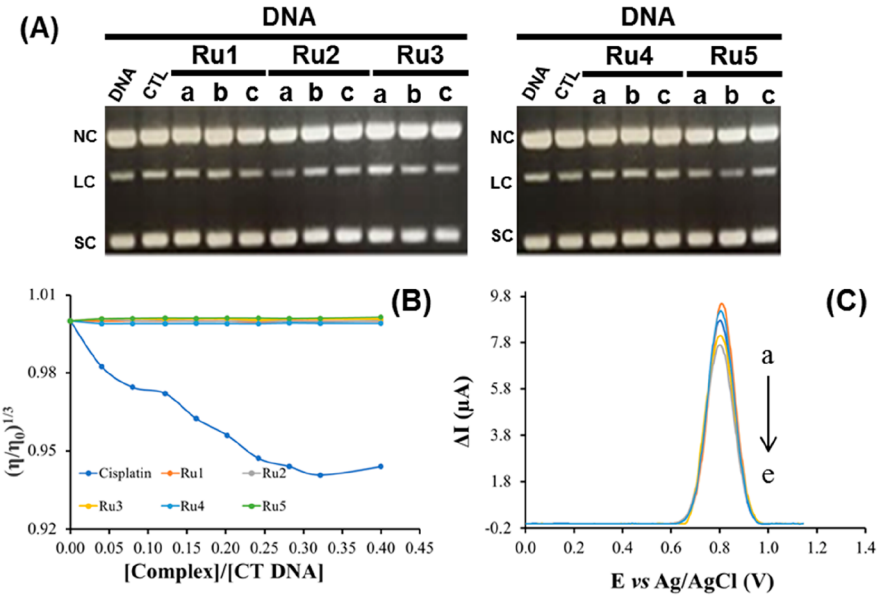

Figure 3. (A) Electrophoresis mobility shift assays of plasmid pBlue-Script KSII(+) in the absence of DNA and CTL and treated with 0.5 (a), 1.0 (b), or 2.0 (c) equiv of **Ru1**−**Ru5**. CTL refers to untreated plasmid in Tris-HCl buffer with 10% DMSO. (B) Effect of increasing concentration of the ruthenium(II) complexes on the relative viscosity of CT DNA. [DNA] = 150 μM. (C) Square-wave voltammograms of 1.0 mM **Ru1** in the absence (a) and presence of DNA at different concentrations: (a) 0, (b) 15, (c) 29, (d) 43, and (e) 57 μM.

complexes containing bipyridine gave IC_{50} values ranging from 0.20 ± 0.03 to 11.74 ± 0.62 μM, whereas the new complexes **Ru1**−**Ru5** afforded IC_{50} values below 1.02 ± 0.09 μM. In contrast, the IC_{50} values for complex [Ru(N-S)$_2$(dppb)] were above 8.80 ± 1.44 μM. This behavior has also been observed for other cancer cell lines. Even if the diphosphine ligands are different in the series of complexes, the presence of the two diphosphine ligands was crucial for the cytotoxic activity of complexes **Ru1**−**Ru5**. We believe that these results stemmed from the lipophilic character of the ruthenium(II) complexes, conferred mainly by the diphosphine ligands. Thus, changing the lipophilicity or charge of the ruthenium(II) complexes, or both, might be an effective way of tuning their cytotoxicity.

Having this in mind, we evaluated the partition coefficient of the ruthenium(II) complexes in water and *n*-octanol. The log *P* values determined for the ruthenium(II) complexes were 0.26 ± 0.04 (**Ru1**), 0.31 ± 0.01 (**Ru2**), 0.24 ± 0.11 (**Ru3**), 0.44 ± 0.02 (**Ru4**), and 0.36 ± 0.10 (**Ru5**). These positive values of log *P* reflected the relative affinity of these complexes for the lipid-like organic phase. Lipophilic compounds are expected to cross biological membranes more easily, which would justify the high cytotoxic activity of the ruthenium(II) complexes. However, on the basis of the aforementioned data, the lipophilicity was not directly correlated with the IC_{50} values of the ruthenium(II) complexes, probably because the lipophilicities of these complexes were practically the same within experimental error. Consequently, other parameters like the presence of peripheral groups in the mercapto ligand may also underline the activity of the ruthenium(II) complexes.

HSA Binding Study by Fluorescence Quenching. The novel anticancer metal therapeutic candidates will probably be applied by an intravenous route, like most commercially available anticancer drugs. In this perspective, pharmacological characterization of ruthenium(II) complexes with the most abundant protein in human plasma, HSA, is of great importance. HSA plays a vital role in drug biodistribution, transport, release, and toxicity. Therefore, we evaluated some aspects of the drug−protein interactions to an initial understanding of drug pharmacokinetics.[12,47−49]

The HSA fluorescence intensity gradually decreased with increasing concentration of the ruthenium(II) complexes, indicating that the microenvironment of the HSA Trp-214 residue was affected (Figure S39). To evaluate the HSA fluorescence quenching mechanism, the Stern−Volmer constant was determined at different temperatures (Table S6). The Stern−Volmer constant values decreased with increasing temperature, indicating that the mechanism of HSA fluorescence quenching was static. Indeed, the bimolecular quenching constant (k_q) values were higher than 1×10^{10} M^{-1} s^{-1}, exceeding the maximum value of the k_q constant for a mechanism to be considered pure dynamic quenching.[50]

We found binding constant values (Table S4) lying between 10^4 and 10^6 M^{-1} for complexes **Ru1**−**Ru5** binding to HSA, which indicated a moderate-to-strong affinity between the species. Furthermore, the number of specific binding sites was approximately 1. Analysis of the thermodynamic parameters with positive ΔH and ΔS values[51] showed that hydrophobic interactions were the main intermolecular forces involved in insertion of the ruthenium(II) complexes into the HSA framework. Negative ΔG values revealed that the HSA−ruthenium(II) complex binding affinities were spontaneous. Thus, the ruthenium(II) complexes would be transported into human plasma by HSA.

Interactions with DNA. To investigate whether DNA is a biological target for the ruthenium(II) complexes, we conducted binding affinity studies by electrophoretic mobility plasmid pBlue-Script KSII(+) in gel agarose (Figure 3A), viscosity (Figure 3B), and square-wave voltammetry (Figures 3C and S40). Compared to untreated plasmid DNA, the patter of electrophoretic mobility of the circular (NC), linear (LC), and supercoiled (SC) conformations of plasmid DNA treated with different concentrations of the ruthenium(II) complexes was not affected (Figure 3A). Moreover, there were no alterations in the DNA viscosity in the presence of ruthenium-

https://doi.org/10.1021/acs.inorgchem.1c01539
Inorg. Chem. 2021, 60, 14174−14189

(II) complexes, at different concentrations, which contrasted with the effects of cisplatin (used as a positive control). Cisplatin significantly decreased the DNA viscosity because of irreversible covalent binding to DNA (Figure 3B). As for the voltammetric assay, the peak potential values corresponding to the Ru^{III}/Ru^{II} couple were shift slightly toward lower potentials, after addition of CT DNA to the solutions of ruthenium(II) complexes (Figures 3C and S40). Increasing the electron density on the Ru^{II} center suggested reversible electrostatic interactions between the negatively charged DNA and the positively charged ruthenium(II) complexes. Therefore, the covalent and intercalation binding modes of the ruthenium(II) complexes to DNA were unlikely. Thus, these experiments indicated that complexes **Ru1**−**Ru5** did not lead to significant conformational altercation in the tertiary and secondary DNA structures. The results were consistent with the structural features of the ruthenium(II) complexes and showed that the DNA binding affinity for the complexes did not depend on the auxiliary mercapto ligands. Also, ruthenium-(II) complexes might not exert their cytotoxic action directly through DNA damage pathways. The "trigger" for cell death could be associated with other biological targets, such as enzymes overexpressed in tumor cells.

Topoisomerase IB Activity. We evaluated hTopIB inhibition at different concentrations of complexes **Ru1**−**Ru5** by supercoiled plasmid DNA relaxation assay (Figure 4). All of the ruthenium(II) complexes inhibited the ability of hTopIB to relax supercoiled plasmid DNA. The inhibition efficacy was concentration-dependent. As shown by the disappearance of several circular DNA forms, **Ru2** (at 100 μM) and **Ru3** (at 6 μM) totally inhibited the hTopIB activity. These results indicated that the hTopIB inhibition by ruthenium(II) complexes is dependent on the auxiliary mercapto ligands. Upon preincubation of the ruthenium(II) complexes with hTopIB, DNA relaxation was efficiently inhibited (Figure S41). After preincubation for 1 min, complexes **Ru1**, **Ru2**, **Ru4**, and **Ru5**, at low concentrations, completely inhibited hTopIB. These results suggested that the ruthenium(II) complexes can act directly on hTopIB, as well as on hTopIB in the presence of DNA (hTopIB-DNA). Complex **Ru3** was the most potent topoisomerase IB inhibitor: it completely inhibited the hTopIB I activity at the lowest concentration among all of the ruthenium(II) complexes. To investigate whether complex **Ru3** disrupts the hTopIB catalytic cycle, we carried out studies on cleavage and religation reactions.

We assayed the kinetics of substrate cleavage in a time-course reaction by using a suicide cleavage substrate, in the presence and absence of complex **Ru3**. The asymmetric CL14/CP25 substrate has its 5′-end radiolabeled at the short strands. The enzyme preferentially cleaves the substrate at the site indicated by the arrow (Figure 5). The cleaved DNA fragments were resolved in a time-course experiment in agarose gel, and the amount of fragment was normalized and plotted as a function of time (Figure 5B). In the case of the negative control (10% DMSO), the kinetics of substrate cleavage by hTopIB was fast and efficient: about 80% of the substrate was cleaved within 45 s. After 20 min, the substrate had been completely cleaved. In contrast, complex **Ru3** totally inhibited the hTopIB catalytic activity in the substrate cleavage.

We studied the religation kinetics by testing the ability of hTopIB toward religate the complementary oligonucleotide R11 to the product of the cleaved substrate (Figure 6) in the absence and presence of complex **Ru3**. Initially, the cleaved

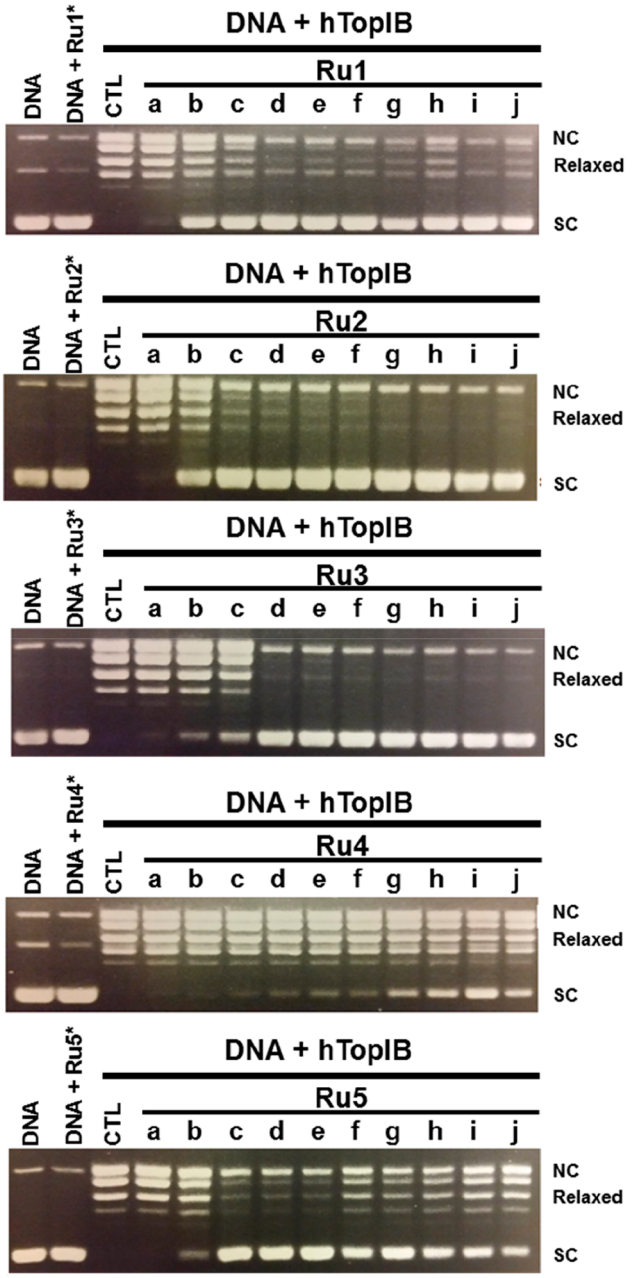

Figure 4. Relaxation of supercoiled plasmid pBlue-Script KSII by topoisomerase IB at different concentrations of complexes **Ru1**−**Ru5**. *Concentration of ruthenium(II) complex of 300 μM. CTL refers to the negative control (10% DMSO). Concentrations (μM) of the ruthenium(II) complexes: (a) 0.75; (b) 1.50; (c) 3; (d) 6; (e) 12.5; (f) 25; (g) 50; (h) 100; (i) 200; (j) 300.

substrate was obtained by incubating the substrate with hTopIB. The percentage of religated substrate was normalized and plotted as a function of time. As expected, hTopIB had a high religation rate, with a plateau being reached within approximately 20 min, with a religation rate of 100% (Figure 6B). The data showed that the presence of complex **Ru3** slowed the religation kinetics compared to the negative control. The presence of complex **Ru3** strongly decreased the rate of substrate religation by hTopIB, with the curve reaching a plateau with approximately 50% religation rate.

https://doi.org/10.1021/acs.inorgchem.1c01539
Inorg. Chem. 2021, 60, 14174−14189

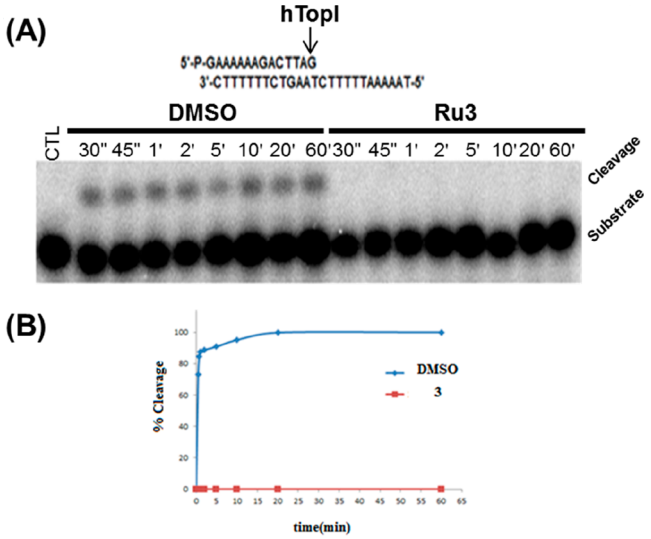

Figure 5. Kinetics of substrate cleavage by hTopIB in the presence of complex **Ru3**. (A) Time course of the CL14-U/CP25 substrate (at the top) cleavage reaction by hTopIB in the presence of complex **Ru3** and 10% DMSO (negative control). CTL represents the DNA strand cleaved by the enzyme at the preferred cleavage site, as indicated by an arrow at the top of the figure. (B) Percentage of cleaved substrate, normalized to the maximum value of the CTL, plotted against time for reaction in the presence of complex **Ru3** and DMSO (10%). The data are the mean ± SD of three independent experiments.

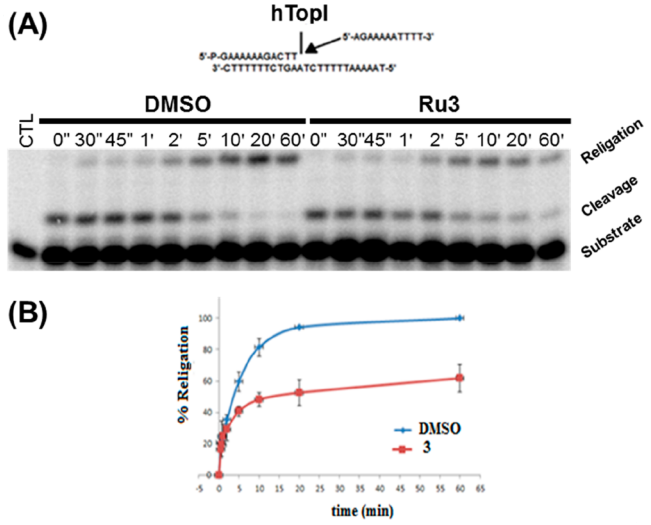

Figure 6. Kinetics of substrate religation by hTopIB in the presence of complex **Ru3**. (A) Time course of the substrate religation reaction by hTopIB in the presence of complex **Ru3** and 10% DMSO (negative control). The substrate was CL14-U/CP25, and the complementary oligonucleotide R11 was used for rewiring (at the top). CTL represents the DNA strand cleaved by hToPIB at the preferred cleavage site, as indicated by an arrow at the top of the figure. (B) Percentage of rewired product, normalized to the maximum value of the CTL, plotted against time for the reaction with complex **Ru3** and 10% DMSO. The data are the mean ± SD of three independent experiments.

Therefore, complex **Ru3** acts as a hTopIB catalytic and poison inhibitor; that is, it is a mixed inhibitor. Complex **Ru3** can act by preventing hTopIB from binding to DNA, thereby inhibiting the cleavage reaction. Also, it can stabilize the intermediate state of the hTopIB-DNA complex in the religation step. Therefore, hTopIB inhibition may consequently lead to cell death from hTopIB-mediated DNA damage.

Molecular Docking Studies of Ru1−Ru5 Complexes with hTopIB and hTopIB-DNA. The molecular docking technique was performed to evaluate the types of interactions between complexes **Ru1−Ru5** and the binding sites of hTopIB and hTopIB-DNA biomolecules.[51] The binding site was defined on the cocrystallized (PDB 1T8I),[52] which on hTopIB consists of the important residues Arg364 and Asp532 and additionally on hTopIB-DNA of the DA113 and DT10 nucleobases. The main data from the molecular docking simulations are shown in Figures S42−S47.

At the molecular level, all complexes exhibited a high affinity for the binding site of free hTopIB through hydrophobic interactions and hydrogen bonds (Table S7). The binding energies were from −29.3 to −32.1 kcal mol^{-1}. First, because the phenyl rings of the dppe ligand are treated as hydrophobic centers, they play an important role in stabilizing the interactions of the complexes in the hydrophobic pocket of topoisomerase IB. Several hydrophobic interactions of the π-alkyl and alkyl types are observed between the phenyl rings of the ruthenium complexes with acid amino residues (Figures 7 and S42−S46 and Table S6). The mercapto ligands also play a relevant role due to hydrogen bonds of the complexes with the biomolecule. In the complexes, the S atom from the mercapto ligands acts as a hydrogen acceptor and the Lys532 residue acts as a H-donor atom.

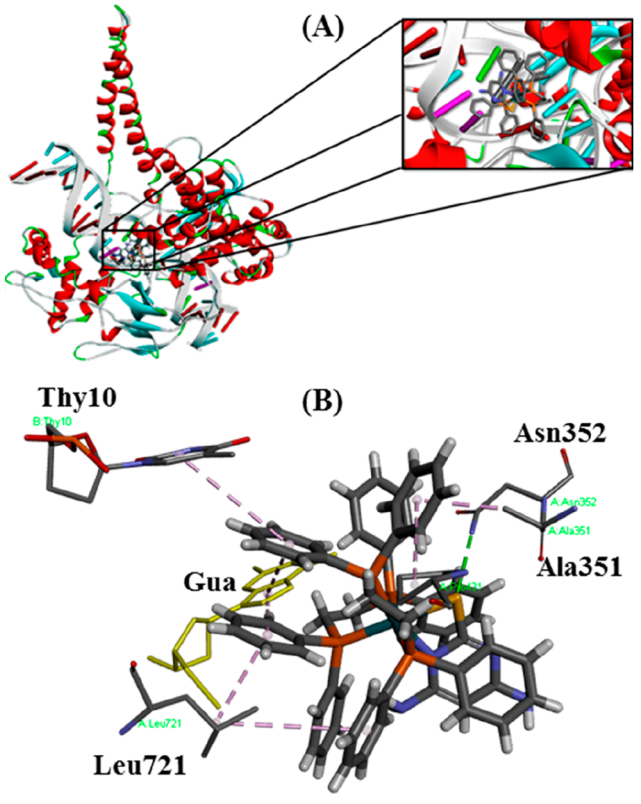

Figure 7. (A) Molecular docking of complex **Ru3** with hTopI-DNA and (B) expansion of the hTopIB-DNA active site with intermolecular interactions.

Molecular docking simulations were also performed using the hTopIB-DNA complex as a receptor in order to evaluate

https://doi.org/10.1021/acs.inorgchem.1c01539
Inorg. Chem. 2021, 60, 14174−14189

the interactions with ruthenium complexes (Figures S42−S47 and Table S8). The best binding poses also demonstrated that complexes **Ru1**−**Ru5** have binding affinities by binding sites on hTopIB-DNA mainly via π-alkyl and alkyl hydrophobic interactions. These interactions occur between the phenyl rings from the dppe ligands and the amino acid residues and nucleotides of hTopIB-DNA. For complexes **Ru2**−**Ru4**, the mercapto ligands also present hydrogen bonds with hTopIB-DNA.

Specifically, compound **Ru3** is tightly fixed around the binding site of free hTopIB (Figure S45) through four alkyl hydrophobic interactions and a hydrogen bond (Table 3). The

Table 3. Docking Interactions between the Complex Ru3 Cleavage/Religation Active Sites from hTop and hTopI-DNA

complex	residue	interaction type	complex Ru moiety
		hTopI and Complex **Ru3**	
Ru3	Arg488	2× alkyl hydrophobic	P-phenyl
	Lys532	hydrogen bond	S-dmp
	Lys532	alkyl hydrophobic	P-phenyl
	Lys493	alkyl hydrophobic	P-phenyl
		hTopI-DNA and Complex **Ru3**	
Ru3	thymine	π-alkyl hydrophobic	P-phenyl
	guanine	π-alkyl/alkyl hydrophobic	P-phenyl
	Leu721	2× alkyl hydrophobic	P-phenyl
	Asp352	hydrogen bond	S-dmp
	Ala351	alkyl hydrophobic	P-phenyl
	Pro431	alkyl hydrophobic	P-phenyl

S atom on the dmp ligand was mapped as a hydrogen acceptor for hydrogen bonding from the NH_2 group on the Arg488 amino acid residue. These interactions are able to stabilize the combination of complexes with hTopIB, inhibiting the binding of the enzyme to DNA. On the other hand, in the hTopIB-DNA species (Figure 7), complex **Ru3** binds to the active site via six hydrophobic interactions and one hydrogen bond. Among them, there are four π-alkyl/alkyl interactions between the phenyl rings of **Ru3** and the amino acid residues from the hTopIB enzyme. Also, there are π-alkyl and alkyl hydrophobic interactions of the diphosphine ligands from **Ru3** with the thymine and guanine moieties of the nucleobases, respectively (Table 3). The molecular docking results demonstrated that complex **Ru3** is able to stabilize the binding sites of both free hTopIB and hTopIB-DNA, which justifies the ability of complex **Ru3** to inhibit the enzymatic activity in the cleavage and religation steps, respectively.

Biological Studies with Complex Ru3. Given that complex **Ru3** is a potent hTopIB inhibitor and, shows excellent cytotoxic activity and selectivity for the cancer lung and breast cell lines, we investigated its ability to inhibit the size and number of cell colonies by clonogenic assay (Figure 8A,B).[53] The long-term survival (Figure S48) of the A549 and MDA-MB-231 cancer cells, and the MRC-5 nontumor cell line was assessed at different concentrations of complex **Ru3**. For the three cell lines, the number and size of the cell colonies decreased upon treatment with complex **Ru3** in a concentration-dependent manner. In the case of the MDA-MB-231 cancer cells treated with complex **Ru3** (Figure 8A), cell survival reduced significantly at the **Ru3** concentrations (0.02 and 0.08 μM) below its corresponding IC_{50}. At a concentration of 0.20 μM, complex **Ru3** completely inhibited formation of

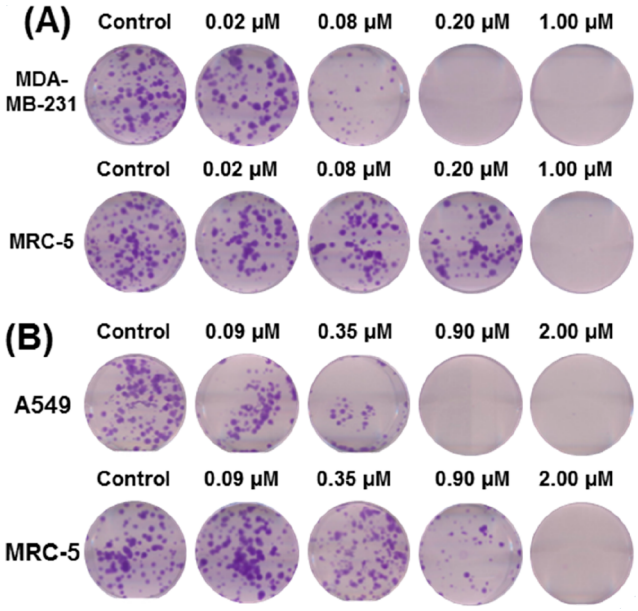

Figure 8. Assessment of the cell survival by clonogenic assay. Representative colony formation images: (A) MDA-MB-231 cancer and MRC-5 nontumor cells after treatment with different concentrations of complex **Ru3**; (B) A549 cancer and MRC-5 nontumor cells after treatment with different concentrations of complex **Ru3**. The negative control group was treated with the vehicle (0.05% DMSO).

the MDA-MB-231 cell colonies, whereas the survival of the MRC-5 nontumor cells was 73% (Figure 8A). However, none of the cells survived at 1.00 μM **Ru3**. Likewise, the number and size of the A549 cancer cell colonies also decreased upon exposure to complex **Ru3** (Figure 8B). At a concentration of 0.9 μM, complex **Ru3** allowed no A549 cancer cells to survive, while the survival of the MRC-5 nontumor cells was 48% (Figure 8B). For both the A459 cancer and MRC-5 nontumor cells, no cell colonies were observed in the presence of 2.0 μM complex **Ru3**. On the basis of this assay, complex **Ru3** exhibited both cytotoxic and cytostatic activity against the tested cell lines. Importantly, the cytotoxic and antiproliferative activity of complex **Ru3** on the MRC-5 nontumor cells was less pronounced compared to its activity against the A549 and MDA-MB-231 cancer cell lines, in accordance with the selectivity results for this complex.

Mutagenic Activity. *Ames Test.* When therapeutic agents bind to DNA, they usually present mutagenicity. Several mutagenic complexes used in cancer treatment (e.g., cisplatin and carboplatin) have their mechanism of action associated with their interaction with DNA.[54] This adverse characteristic is related to the carcinogenicity of such agents. The mutagenicity associated with complex **Ru3** was investigated by the Ames test, in vitro, in the presence and absence of exogenous activation (Table 4). Compared to the negative control group, complex **Ru3** did not increase the average number of revertants in the *Salmonella typhimurium* strains TA98, TA100, TA102, and TA97 at any of the tested concentrations. In contrast, the mean values increased significantly for all of the bacterial strains in the positive control groups. We concluded that complex **Ru3** did not promote gene mutations in the tests with or without metabolic activation for any of the tested bacterial strains. For all of the tested concentrations, the mutagenicity index (MI) was less

https://doi.org/10.1021/acs.inorgchem.1c01539
Inorg. Chem. 2021, 60, 14174−14189

Table 4. Revertants/Plate, Standard Deviation, and MI[a] (in Brackets) in the *S. typhimurium* Strains TA1535 after Treatment with Complex Ru3, with (+S9) and without (−S9) Metabolic Activation

	no. of revertants/plate (MI)[a]			
	TA98		TA100	
treatment (μg plate^{-1})	+S9	−S9	+S9	−S9
negative control[b]	20 ± 3	23 ± 2	111 ± 10	129 ± 15
positive control[c]	878 ± 45 (43.9)	1367 ± 50 (59.4)	1109 ± 55 (9.99)	1374 ± 76 (10.6)
Ru3 (0.78)	19 ± 2 (1.0)	20 ± 5 (0.9)	110 ± 7 (1.0)	124 ± 10 (1.0)
Ru3 (1.56)	18 ± 13 (0.9)	25 ± 4 (1.1)	99 ± 9 (0.9)	128 ± 11 (1.0)
Ru3 (3.12)	18 ± 3 (0.9)	28 ± 2 (1.2)	100 ± 7 (0.9)	127 ± 9 (1.0)
Ru3 (6.25)	20 ± 2 (1.0)	26 ± 6 (1.1)	104 ± 6 (0.9)	127 ± 13 (1.0)
Ru3 (9.37)	19 ± 1 (1.0)	25 ± 3 (1.1)	102 ± 11 (0.9)	124 ± 10 (1.0)
	no. of revertants/plate (MI)[a]			
	TA102		TA97a	
treatment (μg plate^{-1})	+S9	+S9	+S9	+S9
negative control[b]	320 ± 15	359 ± 15	100 ± 10	128 ± 15
positive control[c]	1238 ± 41 (3.9)	1347 ± 50 (26.9)	1031 ± 67 (10.3)	1471 ± 72 (11.5)
Ru3 (0.78)	317 ± 10 (1.0)	358 ± 12 (1.0)	98 ± 19 (1.0)	130 ± 10 (1.0)
Ru3 (1.56)	321 ± 12 (1.0)	356 ± 13 (1.0)	97 ± 17 (1.0)	132 ± 12 (1.0)
Ru3 (3.12)	328 ± 10 (1.0)	360 ± 12 (1.0)	100 ± 11 (1.0)	127 ± 15 (1.0)
Ru3 (6.25)	325 ± 15 (1.0)	359 ± 17 (1.0)	98 ± 14 (1.0)	131 ± 11 (1.0)
Ru3 (9.37)	320 ± 10 (1.0)	347 ± 20 (1.0)	96 ± 15 (1.0)	130 ± 10 (1.0)

[a]MI was also calculated from the average number of revertants per plate with the test complex divided by the average number of revertants per plate with negative control. Values are the mean ± SD. [b]Negative control: DMSO (100 μL plate^{-1}). [c]Positive control: sodium azide (1.25 μg plate^{-1}) in the absence of S9 and c2-anthramine in the presence of S9.

than 2.0, which encourages further studies on their possible uses in anticancer therapy.

Cytokinesis-Block Micronucleus Cytome (CBMN-cyt) Assay. Drug-metabolizing cells, such as cells derived from human liver, are used for the detection of genotoxic compounds. We evaluated the chromosome damage induced by complex **Ru3** by analyzing the frequencies of micronuclei (MNs), nucleoplasmatic bridges (NPBs), and nuclear buds (NBUDs) in binucleated HepG2 cells. The nuclear division index (NDI) was determined by the proportion of mono-, bi-, tri-, or multinucleated cells. The HepG2 cells treated with different concentrations of complex **Ru3** did not differ in terms of the frequencies of MNs, NPBs, NBUDs, and NDI (Table 5) when compared to the negative control group. These results demonstrated that complex **Ru3** did not induce chromosome damage in HepG2 cells under the employed experimental conditions. Doxorubicin, used as a positive control, significantly increased the frequencies of these parameters in the cells, which showed its genotoxicity.

In Vivo Antitumor Assay B16-F10 Cells. The in vivo antitumor activity of complex **Ru3** was evaluated in tumor-bearing C57BL/6 mice engrafted with B16-F10 melanoma cells (Figure 9). The mice were randomly divided into three groups: treated with complex **Ru3**, with cisplatin (positive control), and without treatment (negative control). The doses were administered by intraperitoneal injections for five consecutive days. After treatment for 5 days, the mean tumor mass of the mice of the negative control group was 4.2 ± 0.7 g (Figure 9A). For the mice treated with complex **Ru3** and cisplatin, the mean tumor masses were 0.9 ± 0.2 and 1.5 ± 0.2 g, respectively. The tumor mass growth inhibition rates were 79% and 64% for complex **Ru3** and cisplatin, respectively, compared to the mice of the negative control group. The results demonstrated that complex **Ru3** inhibited tumor development more efficiently than cisplatin. In addition, microscopic analysis revealed a significantly reduced frequency of mitoses in tumor tissue of the mice treated with complex **Ru3** and cisplatin compared to the control group, indicating low proliferative activity of the melanoma cells (Figure 9B).

Furthermore, some toxicological aspects were evaluated in all mouse groups (Figure 9C,D). The group of mice treated with cisplatin exhibited a significant loss of body weight—3.8 ± 0.3 g—compared to healthy mice, while the group of mice treated with complex **Ru3** exhibited no significant alterations in body weight compared to the vehicle and negative control groups. Also, the mean weight of tissues in all of the groups was analyzed (Figure 9D). Weight analysis of the liver, kidneys, spleen, heart, and lungs of the mice treated with complex **Ru3** did not show any significant variations compared to the vehicle control group. For liver weight, the mice treated with cisplatin showed a weight loss of 47% compared to the vehicle control group. These results confirmed complex **Ru3** as a novel anticancer drug candidate for melanoma cancer. This complex reduced B16-F10 cell growth in mice more efficiently than

Table 5. Assessment of Mutagenic Effects of Complex Ru3 on HHO-K1 Cells by Means of CBMN-cyt Assay

	total in 1000 binucleated cells			
treatment	MNs	NPBs	NBUDs	IDN
negative control	3.33 ± 1.56	3.00 ± 0.67	4.67 ± 2.89	1.85 ± 0.05
positive control	59.33 ± 9.55[d]	21.33 ± 5.58[d]	11.33 ± 5.12[d]	1.78 ± 0.83
Ru3 (1.5 μM)	2.00 ± 1.33	5.2 ± 1.00	6.63 ± 1.53	2.00 ± 0.18
Ru3 (3.0 μM)	1.56 ± 0.44	3.3 ± 0.67	1.67 ± 0.89	1.78 ± 0.05
Ru3 (6.0 μM)	1.79 ± 0.89	1.97 ± 0.44	1.00 ± 0.67	1.88 ± 0.11

[a]Values are the mean ± SD. Abbreviations: N, binucleated cell; MN, micronuclei; NPBs, nucleoplasmic bridges; NBUDs, nuclear buds; NDI, nuclear division index. The data are based on three independent experiments. [b]Vehicle negative control: 1.0% DMSO. [c]Positive controls: 0.05 μM doxorubicin; 5 μM aflatoxin B1. [d]Significantly different from the vehicle control ($p < 0.05$).

https://doi.org/10.1021/acs.inorgchem.1c01539
Inorg. Chem. 2021, 60, 14174−14189

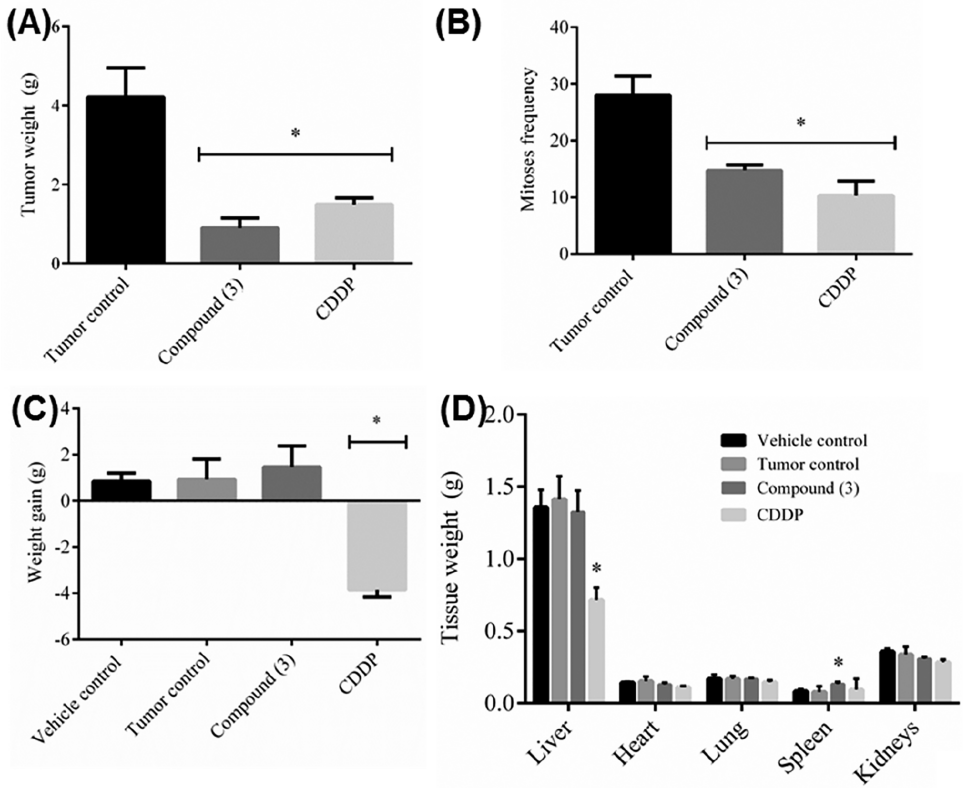

Figure 9. In vivo antitumor activity of complex **Ru3** and respective controls in C57BL/6 mice with melanoma cell xenografts, submitted to treatment for 5 days: (A) tumor weight (g); (B) number of mitoses of the tumor; (C) mean body weight variation; (D) organ weights. Tumor control: with tumor and treated with the vehicle DMSO (5%); cisplatin (5 mg kg^{-1} body weight). *Significantly different from the tumor control group ($p < 0.05$).

cisplatin. As for the analyzed toxicological aspects, complex **Ru3** was advantageous over cisplatin: in contrast to cisplatin, complex **Ru3** did not change the body and tissue weights.

CONCLUSIONS

We have developed new ruthenium(II) complexes of the general formula $[Ru(N\text{-}S)(dppe)_2]PF_6$ obtained from of the precursor *cis*-$[RuCl_2(dppe)_2]$ with five mercapto ligands. The precursor complex by itself already has excellent cytotoxic activity, especially against DU-145, A549, and MDA-MB-231 cancer cell lines, being more active than that cisplatin. Most of the complexes synthesized endowed hydrophobic species with high cytotoxic activity against five cancer cell lines. The IC_{50} values of the complexes are lower than the IC_{50} values of cisplatin against the A549 and MDA-MB-231 cancer cell lines. For the A549 cancer cell line, the IC_{50} value of the complexes is between 288- and 14-fold lower than the IC_{50} value of cisplatin. For the MDA-MB-231 cancer cell line, the IC_{50} value of the complexes is between 81 and 1 times lower compared to the commercial drug. Furthermore, the complexes are more selective for the A549 and MDA-MB-231 cancer cell lines than for nontumoral lung MRC-5 cell line. Complex **Ru5** stands out for being 114 times more active against the A549 tumor cell line than against the MRC-5 nontumor cell line, whereas cisplatin has a MRC-5/A549 selectivity index of 2.08. In general, ruthenium(II) complexes containing two diphosphine ligands and mercapto ligand are highly hydrophobic complexes, which certainly facilitates their cellular uptake. Complexes **Ru1** and **Ru2** are more cytotoxic than complexes **Ru3**−**Ru5**. Structurally, complexes **Ru1** and **Ru2** are characterized by mercapto ligands without functional groups or "electrophilic groups" attached to the rings, whereas complexes **Ru3**−**Ru5** have mercapto ligands with "donor groups" in the mercapto ligand, such as amine and carbonyl moieties.

The complexes bind to DNA through reversible electrostatic interactions, but none of them cause significant damage to the tertiary and secondary DNA structures. Thus, the results suggest that the "trigger" for cell death does not involve the "direct action" of complexes **Ru1**−**Ru5** on DNA. By screening of the complexes with the hTopIB, it was demonstrated that they inhibit the hTopIB catalytic activity in a dose-dependent manner. Specifically, complex **Ru3** at 6 μM completely inhibits hTopoIB. This complex acts not only by preventing the binding of hTopIB to DNA during the cleavage reaction, but also by stabilizing the intermediate state of the hTopIB-DNA complex. In accordance, molecular docking results demonstrated that complexes **Ru1**−**Ru5** exhibit affinity by active sites for both free hTopIB and hTopIB-DNA, which can lead to inhibition of the enzymatic activity. The phenyl rings of the dppe phosphine ligands are responsible for π-alkyl/alkyl hydrophobic interactions and the mercapto ligands for hydrogen bonds. Additionally, the cytotoxic activity of this complex may be related to its interactions with hTopIB.

Complex **Ru3** significantly inhibits melanoma tumor growth in mice, without signs of systemic toxicity. Histopathological analysis revealed that this complex significantly reduces the number of mitoses when compared to the untreated group. In this sense, complex **Ru3** acts by inhibiting cell division in melanoma tumor tissue implanted in mice. Furthermore,

https://doi.org/10.1021/acs.inorgchem.1c01539
Inorg. Chem. 2021, 60, 14174−14189

complex **Ru3** does not promote gene mutations, as evaluated by the Ames test, and does not induce chromosome damage in drug-metabolizing cells. Thus, we hope that the results described herein constitute compelling evidence that the ruthenium(II) diphosphine complexes have therapeutic potential as candidate drugs for cancer treatment, encouraging the advance of in vivo biological assays with this class of complexes.

EXPERIMENTAL SECTION

Instrumentation. The IR spectra were obtained using KBr pellets in a Bomem-Michelson 102 Fourier transform infrared spectrometer in the 4000−200 cm^{-1} region. Cyclic voltammetry experiments were performed in a BAS model 100B electrochemical analyzer and carried out at room temperature. The typical conditions were 0.10 mol L^{-1} Bu_4NClO_4 (TBAP) as a supporting electrolyte in CH_2Cl_2 and an electrochemical cell with a three-electrode system, where a glassy carbon was used as the working electrode, Ag/AgCl as the reference electrode, and a platinum plate as the auxiliary electrode. Elemental analyses were performed in the Microanalytical Laboratory at the Universidade Federal de São Carlos, São Carlos, Brazil, with an EA 1108 CHNS microanalyzer (Fisons Instruments). Conductivity values were obtained, at room temperature, using 1.0×10^{-3} M solutions of the complexes in CH_2Cl_2 in a Meter Lab CDM2300 instrument. $^{31}P\{^1H\}$, ^1H, COSY ($^1H-^1H$), $^{13}C\{^1H\}$, and HSQC ($^1H-^{13}C$) NMR were recorded on a Bruker DRX 400 MHz using chemical shifts, which are reported in relation to H_3PO_4, 85% CH_2Cl_2/D_2O, or DMSO-d_6. The UV−vis spectra of the complexes were recorded in CH_2Cl_2 on a Hewlett-Packard 8452A diode array.

X-ray Crystallography. All single crystals for complexes **Ru1**, **Ru2**, **Ru4**, and **Ru5** were obtained from solvent evaporation [a 1:1 (v/v) dichloromethane and methanol mixture]. X-ray diffraction was carried out at room temperature using a Bruker AXS-Mach3 diffractometer and an APEX II CCD area detector with Mo Kα radiation (λ = 0.71073 Å). All crystal structures were resolved by direct methods, and the models were refined by full-matrix least squares on F^2 using *SHELX*.[55] Anisotropic displacement parameters were applied for Ru, P, S, C, N, O, and F atoms. H atoms were located at their positions and refined with the appropriate riding model, considering the C−H distance fixed as 0.93 and 0.97 Å for C−H aromatic and methylene bonds, respectively, with $U_{iso}(H) = 1.2U_{eq}(C_{aromatic}/C_{methylene})$. Summaries of the crystal data collection procedures and refinement results for complexes are given in Tables S1 and S2. The representation of the structure was drawn with the *Mercury 4.0* program.[56]

Materials for Synthesis. Reactions and chemicals were handled under an argon atmosphere. Solvents were purified by standard methods. All chemicals used were of reagent grade or comparable purity. $RuCl_3 \cdot 3H_2O$, 1,2-bis- (diphenylphosphino)ethane (dppe) ligand; 1,3-thiazolidine-2-thione (mtz); mercapto-1-methylimidazole (mmi); 4,6-diamino-2-mercapto-pyrimidine (dmp); 6-mercaptopyridine-3-carboxylic acid (mpca) and 2-mercapto-4(3H)-quinazoline (2mq) ligands were used as received from Sigma-Aldrich. The *cis*-$[RuCl_2(dppe)_2]$ compound, used as a precursor for the synthesis of complexes **Ru1**−**Ru5**, was prepared according to published procedures.[57]

Synthesis of Complexes Ru1−Ru5. The $[Ru(N\text{-}S)(dppe)_2]PF_6$ complexes were obtained from the *cis*-$[RuCl_2(dppe)_2]$ precursor. In a Schlenk flask with a mixture of 15 mL of methanol and 15 mL of CH_2Cl_2 previously degassed, 0.12 mmol of the respective mercapto ligand was added (mtz = 0.014 g; mmi = 0.014 g; dmp = 0.023 g; mpca = 0.019 g, and 2mq = 0.021 g) along with 32 μL (24 mmol) of triethylamine. Posteriorly, 0.10 mmol (0.097 g) of the precursor *cis*-$[RuCl_2(dppe)_2]$ and 0.13 mmol (0.024 g) of KPF_6 were added to the flask. The system was kept under stirring and reflux for approximately 12 h. The volume of the solution was reduced to approximately 2 mL, and water was added to precipitate a yellow powder. The precipitate was filtered off, washed with water and ethyl ether, and dried under vacuum.

[Ru(mtz)(dppe)$_2$]PF$_6$ ***(Ru1)***. Yield: 89%. Anal. Calcd for $C_{57}H_{58}F_6NP_5RuS_2$ [exptl (calcd)]: C, 57.05 (56.89); H, 4.66 (4.51); N, 1.09 (1.21); S, 5.65 (5.52). Molar conductance (μS cm^{-1}, CH_2Cl_2): 50.2. IR (cm^{-1}): ν(C−H) 3065/3053, $\nu(CH_2)$ 2949/2854, ν(C=N) 1584, ν(C=C + C=N) 1514, ν(C−S) 1268, ν(P−C_{ring}) 1093, $\nu(PF_6^-)$ 842, 739, $\delta(PF_6)$ 559, ν(P−C) 522, ν(Ru−S) 426, ν(Ru−N) 406. UV−vis [CH_2Cl_2; λ/nm (ε/M^{-1} cm^{-1})]: 262 (69298; IL), 374 (2816; TCML). $^{31}P\{^1H\}$ NMR (161.98 MHz, CH_2Cl_2/D_2O): δ 57.2 (1P, ddd, $^2J_{PP}$ = 304.5, 19.4, and 13.0 Hz), 47.8 (1P, ddd, $^2J_{PP}$ = 22.7, 19.4, and 9.7 Hz), 45.6 (1P, ddd, $^2J_{PP}$ = 304.5, 25.9, and 9.7 Hz), 39.5 (1P, ddd, $^2J_{PP}$ = 25.9, 22.7, and 13.0 Hz), −144.40 (1P, hept, $^2J_{PF}$ = 710.7 Hz, PF_6^-).

[Ru(mmi)(dppe)$_2$]PF$_6$ ***(Ru2)***. Yield: 95%. Anal. Calcd for $C_{59}H_{59}F_6N_4P_5RuS$ [exptl (calcd)]: C, 58.41 (58.13); H, 4.89 (4.70); N, 2.54 (2.42); S, 2.77 (2.53). Molar conductance (μS cm^{-1}, CH_2Cl_2): 51.4. IR (cm^{-1}): ν(C−H) 3140/3055, $\nu(CH_2)$ 2948/2848, ν(C=N) 1587, ν(C=C + C=N) 1524, ν(C−S) 1283, ν(P−C_{ring}) 1092, $\nu(PF_6^-)$ 844, $\delta(PF_6^-)$ 556, ν(P−C) 524, ν(Ru−S) 425, ν(Ru−N) 402. UV−vis [CH_2Cl_2; λ/nm (ε/M^{-1} cm^{-1})]: 262 (53372; IL), 354 (1244; TCML). $^{31}P\{^1H\}$ NMR (162 MHz, CH_2Cl_2/D_2O): δ 59.2 (1P, ddd, $^2J_{PP}$ = 299.6, 19.4, and 16.2 Hz), 55.9 (1P, ddd, $^2J_{PP}$ = 24.3, 19.4, and 14.6 Hz), 53.4 (1P, ddd, $^2J_{PP}$ = 299.7, 24.3, and 14.6 Hz), 52.8 (1P, ddd, $^2J_{PP}$ = 24.3, 19.4, and 13.0 Hz), −144.40 (1P, hept, $^2J_{PF}$ = 710.7 Hz, PF_6^-).

[Ru(dmp)(dppe)$_2$]PF$_6$ ***(Ru3)***. Yield: 94%. Anal. Calcd for $C_{58}H_{59}F_6N_4P_5RuS$ [exptl (calcd)]: C, 56.50 (56.81); H, 4.49 (4.51); N, 4.62 (4.73); S, 2.53 (2.71). Molar conductance (μS cm^{-1}, CH_2Cl_2): 52.54. IR (cm^{-1}): $\nu(NH_2)$3494/3394, ν(C−H) 3183/3051, $\nu(CH_2)$ 2921/2852, ν(C=N) 1585, ν(C=C + C=N) 1538, ν(C−S) 1248, ν(P−C_{ring}) 1160, $\nu(PF_6^-)$ 841, $\delta(PF_6^-)$ 559, ν(P−C) 518, ν(Ru−S) 406, ν(Ru−N) 375. UV−vis [CH_2Cl_2; λ/nm (ε/M^{-1} cm^{-1})]: 268 (94476, IL), 324 (12130; TCML). $^{31}P\{^1H\}$ NMR (162 MHz, CH_2Cl_2/D_2O): δ 58.9 (1P, ddd, $^2J_{PP}$ = 285.0, 24.3, and 13.0 Hz), 56.5 (1P, ddd, $^2J_{PP}$ = 24.3, 24.3, and 16.2 Hz), 52.6 (1P, ddd, $^2J_{PP}$ = 285.0, 19.4, and 16.2 Hz), 52.0 (1P, ddd, $^2J_{PP}$ = 24.3, 19.4, and 13.0 Hz), −144.40 (1P, hept, $^2J_{PF}$ = 710.7 Hz, PF_6^-).

[Ru(mpca)(dppe)$_2$]PF$_6$ ***(Ru4)***. Yield: 92%. Anal. Calcd for $C_{60}H_{58}F_6NO_2P_5RuS$ [exptl (calcd)]: C, 58.38 (58.20); H, 4.41 (4.38); N, 1.26 (1.17); S, 2.82 (2.68). Molar conductance (μS cm^{-1}, CH_2Cl_2): 52.8. IR (cm^{-1}): ν(C−H) 3153/3051, $\nu(CH_2)$ 2921/2850, ν_{as}(COOH) 1710, ν(C=N) 1587, ν(C=C + C=N): 1534, ν_s(COOH) 1358, ν(C−S) 1254, ν(P−C_{ring}) 1158, $\nu(PF_6^-)$ 843, $\delta(PF_6^-)$ 557, ν(P−C) 522, ν(Ru−S) 411, ν(Ru−N) 377. UV−vis [CH_2Cl_2; λ/nm (ε/M^{-1} cm^{-1})]: 264 (86566; IL), 382 (11660; TCML). $^{31}P\{^1H\}$ NMR (162 MHz, CH_2Cl_2/D_2O): δ 62.2 (1P, ddd, $^2J_{PP}$ = 278.6, 19.4, and 14.6 Hz), 51.0 (1P, ddd, $^2J_{PP}$ = 19.4, 19.4, and 8.1 Hz), 50.1 (1P, ddd, $^2J_{PP}$ = 278.6, 22.7, and 8.1 Hz), 47.7 (1P, ddd, $^2J_{PP}$ = 22.7, 19.4, and 14.6 Hz), −144.40 (1P, hept, $^2J_{PF}$ = 710.7 Hz, PF_6^-).

[Ru(2mq)(dppe)$_2$]PF$_6$ ***(5)***. Yield: 82%. Anal. Calcd for $C_{62}H_{59}F_6N_2OP_5RuS$ [exptl (calcd)]: C, 59.08 (59.07); H, 4.49 (4.38); N, 2.33 (2.30); S, 2.83 (2.63). Molar conductance (μS cm^{-1}, CH_2Cl_2): 55.2. IR (cm^{-1}): ν(C−H) 3144/3051, $\nu(CH_2)$ 2925/2852, ν(C=O) 1653, ν(C=N) 1586, ν(C=C + C=N) 1530, ν(C−S) 1243, ν(P−C_{ring}) 1097, $\nu(PF_6)$ 841, $\delta(PF_6)$ 555, ν(P−C) 525, ν(Ru−S) 425, 409, ν(Ru−N) 377. UV−vis [CH_2Cl_2; λ/nm (ε/M^{-1} cm^{-1})]: 272 (51927; IL), 318 (12485; TCML), 344 (11832; TCML). $^{31}P\{^1H\}$ NMR (162 MHz, CH_2Cl_2/D_2O): δ 57.2−56.5 (2P, multiplet), 53.7−53.0 (1P, multiplet), 52.8−52.2 (1P, multiplet), −144.40 (1P, hept, $^2J_{PF}$ = 710.7 Hz, PF_6^-).

Water/*n*-Octanol Distribution Coefficient (log *P*). Water−octanol partition coefficients were determined using the shake-flask method.[58] A total of 1 mg of each complex was solubilized in 100 μL of DMSO and posteriorly diluted in a mixture of equal volumes of water (750 μL) and *n*-octanol (750 μL). The solutions were continuous shaken for 24 h at 1000 rpm and 37 °C. Then the samples were centrifuged for 5 min at 300 rpm, and the organic and aqueous phases were separated. The concentration of drug in each phase was

https://doi.org/10.1021/acs.inorgchem.1c01539
Inorg. Chem. 2021, 60, 14174−14189

measured spectrophotometrically in order to determine the log P values = [complex(in n-octanol)]/[complex(in water)]. The experiments were carried out in triplicate.

In Vitro Assay. *Cell Culture.* The ruthenium complexes were assayed against human breast cancer cells MCF-7 (ATCC No. HTB-22) and MDA-MB-231 (ATCC No. HTB-26), the human lung tumor line A549 (ATCC No. CCL-185), the human prostate DU-145 (ATCC No. HTB-81), the human hepatocellular carcinoma HepG2, and the normal cell line MRC-5. The cells were routinely maintained with Dulbecco's modified Eagle's medium (DMEM; for HepG2, A549, and MRC-5) or RPMI 1640 (for MCF-7 and DU145), supplemented with 10% fetal bovine serum (FBS), at 37 °C in a humidified 5% CO_2 atmosphere.

Cytotoxicity Assay. The cytotoxic activity of the complexes on cell lines was assessed by 3-(4,5-dimethylthiazol-2-yl)-2,5-diphenyltetrazolium bromide (MTT) assay.[59] Cells (1.5×10^4 well^{-1}) were seeded in 200 μL of a complete medium in 96-well plates (Corning Costar). Each complex was dissolved in sterile DMSO (from 40 to 0.01 mM). A total of 1 μL of each complex sample was added to 200 μL of the medium. Cells were exposed to the complex for a 48 h period. Posteriorly for 48 h, 50 μL of MTT (1 mg mL^{-1}) was added to each well. Cells were incubated again for 4 h, the medium was removed, and formazan crystals were solubilized in isopropyl alcohol. The conversion of MTT to formazan by metabolically viable cells was spectrophotometrically monitored by an automated microplate reader at 540 nm. The percent cell viability was calculated by dividing the average absorbance of cells treated with a ruthenium complex (**Ru1**−**Ru5**) by that of the control; The percent cell viability versus drug concentration (logarithmic scale) was plotted to determine IC_{50} (drug concentration at which 50% of the cells are viable relative to the control), with its estimated error derived from an average of three trials.

Clonogenic Survival Assay. For clonogenic survival assay, the breast cancer strain MDA-MB-231, lung cancer A549, and normal lung cancer strain MRC-5 were used. A total of 300 cells were cultured per well in a six-well plate. After 24 h, with the cells already adhered, they were treated with different concentrations of the selected complex. The concentrations (negative control; $^1/_2 \times IC_{50}$, IC_{50}, and $2 \times IC_{50}$) used were determined from the IC_{50} value of complex **Ru3** in the cancer cell lines. The plates were stored in an oven (37 °C/5% CO_2) for 48 h. Then the culture medium (4 mL) was changed and incubated for another 10 days in an oven. After this period, the culture medium was discarded, and the plates were washed with phosphate saline buffer (PBS). The colonies formed were fixed with a methanol/acetic acid solution (3:1) for 5 min and stained with violet crystal 0.5% water for 25 min. After this period, the plates were washed with water and dried at room temperature. Then the number of colonies formed was counted. The test was performed in triplicate.

Complex/DNA Binding Experiments. *Interaction Study of Ruthenium Complexes and Calf-Thymus DNA (CT-DNA) by Viscosity.* Viscosity measurements were carried out using an Ostwald viscometer immersed in a water bath maintained at 25 °C. The DNA concentration in buffer Tris-HCl was kept constant in all samples (150 μM), while the complex concentration was increased from 0 to 60 μM. In the assay, the percent DMSO was also kept constant. The flow time was measured at least five times with a digital stopwatch, and the mean value was calculated. Data are presented as $(\eta/\eta_0)^{1/3}$ versus the [complex]/[DNA] ratio, where η and η_0 are the specific viscosities of DNA in the presence and absence of the complex, respectively. The values of η and η_0 were calculated using the expression $(t - t_{DNA})/t_{DNA}$, where t is the observed flow time and t_{DNA} is the flow time of the DNA in buffer (DMSO).[60]

Interaction Study of Ruthenium Complexes and CT-DNA by Square-Wave Voltammetry. The complex/CT-DNA interaction studies were performed by square-wave voltammetry. The complex/CT-DNA interaction studies were carried out in a Tris-HCl buffer (pH 7.4) and 30% DMSO. Titration was performed by adding 30 μL aliquots of CT-DNA (0−120 μL; stock solution 1.00 mM) to an electrochemical cell, containing 2 mL of a 1.00 mM complex solution. The final concentrations of CT-DNA were 0, 15, 29, 43, and 57 μM. In this condition, any denaturation of the DNA was observed, and no change in the UV−vis spectra of the solution was detected for at least 1 h.

Interaction Study of Ruthenium Complexes and CT-DNA by Agarose Gel Electrophoresis. Agarose gel electrophoresis studies were performed by incubating 1 μL (0.25 μg μL^{-1}) of pBlue-Script KSII(+) plasmid DNA with 1 μL of stock solution (in DMSO) of different concentrations of the complexes and 28 μL of a Tris-HCl buffer, resulting in 30 μL of final volume. The concentrations of the complexes in the final solutions were after incubation at 37 °C for 20 h, and 20 μL of each sample was run in a 1% agarose gel at 30 V for 18 h using a Tris-borate−ethylenediaminetetraacetic acid (EDTA) buffer and stained with ethidium bromide (5 μL of ethidium bromide per 50 mL of agarose gel mixture). Samples of free DNA and DNA + DMSO (3.3%) were used as controls. The DNA bands were visualized in a UV-light transilluminator (ChemiDocMP, Bio-Rad).

HSA Binding Experiments. Fluorescence spectroscopy is an effective method for exploring the interactions between small molecules and macromolecules. The fluorescence of HSA comes from its tryptophan, tyrosine, and phenylalanine residues, where the latter two contribute to its fluorescence to only a minor extent.[61]

The protein interaction was examined in 96-well plates used for fluorescence assays. HSA (5.0 μM) was prepared by dissolving the protein in Tris-HCl at pH 7.4, and the complexes were dissolved in sterile DMSO. For the fluorescence measurements, the HSA concentration (950 μL) in the buffer Tris-HCl was kept constant in all samples, while the complex concentration (50 μL) was increased by 2.5, 5.0, 7.5, 10.0, 12.5, 15.0, 17.5, and 20.0 μM, and quenching of the emission intensity of the HSA tryptophan residues at 305 nm (excitation wavelength of 270 nm) was monitored at different temperatures (298 and 310 K). The experiments were carried out in triplicate and analyzed using the classical Stern−Volmer equation as follows:[62]

$$F_0/F = 1 + K_q\tau_0[Q] = 1 + K_{SV}[Q] \quad (1)$$

where F_0 and F are the fluorescence intensities in the absence and presence of quencher, respectively, [Q] is the quencher concentration, and K_{SV} is the Stern−Volmer quenching constant, which can be written as $K_q = K_{SV}/\tau_0$, where K_q is the bimolecular quenching rate constant and τ_0 is the average lifetime of the fluorophore in the absence of quencher (6.2×10^{-9} s). Therefore, eq 1 was applied to determine K_{SV} by linear regression of a plot of F_0/F versus [Q].

The binding constant (K_b) and number of complexes bound to HSA (n) were determined by plotting the double-logarithmic graph of the fluorescence data using eq 2 as follows:[63]

$$\log[(F_0 - F)/F] = \log K_b + n \log [Q] \quad (2)$$

The thermodynamic parameters were calculated from eqs 3 and 4:

$$\ln(K_2/K_1) = [(1/T_1) - (1/T_2)]\Delta H/R \quad (3)$$

$$\Delta G = -RT \ln K = \Delta H - T\Delta S \quad (4)$$

where K_1 and K_2 are the binding constants at temperatures T_1 and T_2, respectively, and R is the gas constant.

Topoisomerase IB Assays. *Purification of hTopIB.* hTopIB was expressed by the galactose inducible promoter in a multicopy plasmid, YCpGAL1-e-wild and YCpGAL1-e-Y723F, used for the transformation of EKY3 cells, as described previously.[64] The epitope-tagged constructs contain the N-terminal sequence FLAG: DYKDDDY (indicated with "e"), recognized by the M2 monoclonal antibody. Purification was carried out using an ANTI-FLAG M2 affinity gel column (Sigma-Aldrich). The FLAG-fusion topoisomerase IB was eluted by competition with five column volumes of a solution containing a 100 μg mL^{-1} FLAG peptide in 50 mM Tris-HCl and 150 mM KCl (pH 7.4). Glycerol was added to each fraction up to a final concentration of 40%. All of the fractions were stored at −20 °C. The integrity of the protein was verified by immunoblot assay. The purified protein was resolved on sodium dodecyl/sulfate polyacrylamide gel electrophoresis (SDS-PAGE), transferred to a nitrocellulose membrane, and immunoblotted with a specific monoclonal antibody

https://doi.org/10.1021/acs.inorgchem.1c01539
Inorg. Chem. 2021, 60, 14174−14189

(Sigma A9469). An immunoreactive band, corresponding to topoisomerase I, was detected with a 5-bromo-4-chloro-3-indolyl phosphate/nitro blue tetrazolium substrate (Sigma B3804).

Topoisomerase IB Activity In Vitro: DNA Relaxation Assay. The TopIB activity was assayed by preparing the samples with 1 μL (0.25 μg μL^{-1}) of pBlue-Script KSII(+) plasmid DNA, 1 μL of stock solution (in DMSO) of different concentrations of the complexes and 28 μL of reaction buffer (20 mM Tris-HCl, 0.1 mM EDTA, 10 mM $MgCl_2$, 50 μg mL^{-1} acetylated BSA, and 150 mM KCl, pH 7.4), resulting in 30 μL of final volume. The concentrations of the complexes in the final solutions were 0.75, 1.5, 3.0, 6.0, 12.5, 25.0, 50.0, 100.0, 200.0, and 300.0 μmol L^{-1}. The reaction was incubated for 30 min at 37 °C and interrupted by the addition of 7.5 μL of SDS 4X STOP (25% Ficol 400, 2.5% SDS, 25 mM EDTA, 0.03% bromophenol blue, and 0.03% xylenocyanol). Samples were electrophoresed in 1% agarose gel in 50 mM Tris, 45 mM boric acid, and 1 mM EDTA. The gel was stained with ethidium bromide (5 μg mL^{-1}), destained with water, and photographed under UV illumination. Wherever indicated, the enzyme and inhibitor were preincubated at 37 °C for 5 min before the DNA substrate was added. Assays were performed at least three times, but only one representative gel is shown.

Cleavage Kinetics. The oligonucleotide CL14 (5′-GAAAAAA-GACTTAG-3′), radio-labeled with [γ-^{32}P] adenosine triphosphate (ATP) at its 5′ end, and the CP25 complementary strand (5′-TAAAAATTTTTCTAAGTCTTTTTTC-3′), phosphorylated at its 5′ end, with unlabeled ATP, were annealed at a 2-fold molar excess of CP25 over CL14, creating the so-called "suicide substrate", which contains only a partial duplex. The suicide cleavage reactions were carried out by incubating 20 nM suicide substrate with the enzyme in a reaction buffer at 37 °C and in the presence of 25 μM complex. DMSO (10%) was added to the no-drug control. Before the enzyme was added, a 5 μL sample of the reaction mixture was removed and used as the control. At different time points, 5 μL aliquots were removed and the reactions stopped with 0.5% SDS. After the ethanol precipitation, samples were resuspended in 6 μL of 1 μg mL^{-1} trypsin and incubated at 37 °C for 1 h. Samples were analyzed using denaturing urea/poly acrylamide gel electrophoresis.

Religation Kinetics. A suicide CL14/CP25 substrate (20 nM), prepared as above, was incubated with the topoisomerase IB enzyme for 30 min at 37 °C in a reaction buffer. A 5 μL aliquot of the reaction mixture was removed and used as the zero time point. Religation reactions were initiated by adding a 200-fold molar excess of R11 oligonucleotide (5′-AGAAAAATTTT-3′) over the duplex CL14/CP25 in the presence or absence of 25 μM complex **Ru3**. Moreover, 5 μL aliquots were removed, and the reactions were stopped with 0.5% SDS at different times. Afterward, ethanol precipitation samples were resuspended in 5 μL of 1 μg mL^{-1} trypsin and incubated at 37 °C for 1 h. Samples were analyzed by denaturing urea/polyacrylamide gel electrophoresis. The experiment was replicated three times, and a representative gel is shown.

Molecular Docking Procedure. The docking simulations were implemented using the tools *GOLD v 5.8.0* program.[65] The structure of the human DNA topoisomerase I in complex with different ruthenium complexes was downloaded from the Protein Data Bank (PDB 1T8I),[52] removing the ligant molecule before starting the docking calculation and making a note coordinates of binding site. In the preparation of protein for use in optimization calculations, the *protein-preparation* wizard in *Maestro*[66] was used in this study. The validation study was carried out using the *Chemscore* and *Goldscore* functions for pose selection. The prepared protein and results were visualized and analyzed using *Biovia Discovery Studio Visualizer*.[67]

Mutagenicity Assays. *Ames Test.* The mutagenic activity was evaluated by the salmonella/microsome assay, using the *S. typhimurium* tester strains TA98, TA100, TA97a, and TA102, kindly provided by Dr. B. N. Ames (Berkeley, CA), with (+S9) and without (−S9) metabolization, by the preincubation method.[68] To determine the mutagenic activity, five different concentrations of complex **Ru3** (0.78−75 μg $plate^{-1}$), diluted in DMSO, were assayed. The concentrations of the complex were selected on the basis of a preliminary toxicity test. In all subsequent assays, the upper limit of the dose range tested was either the highest nontoxic dose or the lowest toxic dose determined in this preliminary assay. All experiments were analyzed in triplicate.

The results were analyzed using the statistical software package *Salanal 1.0* (Monitoring Systems Laboratory, U.S. Environmental Protection Agency, Las Vegas, NV, from the Research Triangle Institute, Research Triangle Park, NC), adopting the Bernstein et al. model.[69] The data (revertants/plate) were assessed by analysis of variance (ANOVA), followed by linear regression. MI was also calculated for each concentration tested, which was the average number of revertants per plate with the test complex divided by the average number of revertants per plate with the negative control. A test solution was considered mutagenic when a dose−response relationship was detected and a 2-fold increase in the number of mutants (MI > 2) was observed for at least one concentration.[68] The standard mutagens used as positive controls in experiments without a S9 mix were 4-nitro-*o*-phenylenediamine (NOPD; 10 mg $plate^{-1}$) for TA98 and TA97a, sodium azide (1.25 μg $plate^{-1}$) for TA100, and mitomycin (0.5 μg $plate^{-1}$) for TA102. In experiments with S9 activation, 2-anthramine (1.25 μg $plate^{-1}$) was used for TA98, TA97a, and TA100, and 2-aminofluorene (10 μg $plate^{-1}$) for TA102. DMSO (100 μL $plate^{-1}$) served as the (solvent) negative control.

CBMN-cyt Assay. The mutagenicity was evaluated as described by Fenech.[70] Three different concentrations (IC_{50} and two lower concentrations) were used for CBMN-cyt analysis. A total of 5 × 10^5 HepG2 cultures, as previously described, were incubated in 25 cm^2 culture flasks for 24 h and then treated with three different concentrations of the ruthenium complexes or 0.05 μM doxorubicin. After 20 h of treatment (44 h after initiation of the culture), the cells were washed with PBS, the culture media were changed, and cytochalasin B (final concentration of 3.0 μg mL^{-1}) was added. The cells were then incubated for an additional 28 h, harvested, treated with a cold hypotonic solution (0.01% sodium citrate), and fixed with formaldehyde and methanol/acetic acid (3:1). The slides were stained immediately before analysis using 40 μg mL^{-1} acridine orange, and the binucleated cells with 1−4 MN were scored at 1000× magnification. Additionally, the frequencies of NPBs and NBUDs were evaluated using the criteria of Fenech et al.[41] The NDI was also calculated to evaluate the altered mitotic activity and/or cytostatic effects according to eq 5:[71]

$$\mathrm{NDI} = (\mathrm{M1} + 2\mathrm{M2} + 3\mathrm{M3} + 4\mathrm{M4})/N \quad (5)$$

where M1, M2, M3, and M4 are the number of cells with one, two, three, and four nuclei and N is the number of cells assayed. A total of 500 cells per treatment were analyzed or NDI calculated and 1000 binucleated cells for the MN, NPB, and NBUD frequencies. A total of three independent experiments were performed.

In Vivo Assay. *Antitumor Assay Using Syngeneic Murine Melanoma Tumor Model.* In vivo studies were carried out using treatment protocols approved by the Ethics Committee on Animal Use of the University of Franca (No. 2639070412). Male C57BL/6 mice, weighing 25−30 g, were obtained from the animal house of the University of São Paulo, Ribeirão Preto Campus, São Paulo, Brazil. The B16-F10 cell line (murine melanoma) was maintained in a RPMI culture medium (Sigma-Aldrich), supplemented with 10% FBS (Nutricell), 1.2 g mL^{-1} sodium bicarbonate (Sigma-Aldrich), 0.1 g mL^{-1} streptomycin (Sigma-Aldrich), and 0.06 g mL^{-1} penicillin (Sigma-Aldrich) in a 5% CO_2/air atmosphere at 37 °C. The B16-F10 cells were counted, and their viability was assessed in a Muse Cell Analyzer (Merck). The procedures for obtaining the tumors, as well as the experimental design, were conducted according to Carnizello et al.[72]

The groups of animals with tumor induction were divided as follows: tumor control (5% DMSO; Sigma-Aldrich), compound **Ru3** (5 mg kg^{-1} body weight), and cisplatin (5 mg/ kg^{-1} body weight). A vehicle control group (without tumor and treated with 5% DMSO) was also included.

The tumor growth inhibition rate (TGIR) was calculated by eq 7, as described Qin et al.:[73]

https://doi.org/10.1021/acs.inorgchem.1c01539
Inorg. Chem. 2021, 60, 14174−14189

$$\text{TGIR} = \frac{\text{tumor weight of tumor control} - \text{tumor weight of treatment}}{\text{tumor weight of tumor control}} \times 100 \quad (7)$$

Mice were euthanized on day 6, 24 h after the last treatment. The liver, kidneys, spleen, heart, and lungs were collected and weighed to evaluate the toxicological potential of the treatments. For evaluation of the antitumor activity, the tumors were collected, weighed, and stored for subsequent histopathological analysis. For this, the excised tumors were fixed in 10% neutral formalin and embedded in paraffin blocks. Five segments (5 μm thick) were cut from random parts of each tumor tissue, and the sections were dewaxed and stained with hematoxylin and eosin. Five random fields were analyzed under a microscope regarding the number of mitoses in 400× magnification, for a total of 25 areas per group.

■ ASSOCIATED CONTENT

Supporting Information

The Supporting Information is available free of charge at https://pubs.acs.org/doi/10.1021/acs.inorgchem.1c01539.

Figures and tables providing IR, UV−vis, and NMR spectra, cyclic voltammetry, and X-ray crystallographic data of the complexes (PDF)

Accession Codes

CCDC 2079011−2079014 contain the supplementary crystallographic data for this paper. These data can be obtained free of charge via www.ccdc.cam.ac.uk/data_request/cif, or by emailing data_request@ccdc.cam.ac.uk, or by contacting The Cambridge Crystallographic Data Centre, 12 Union Road, Cambridge CB2 1EZ, UK; fax: +44 1223 336033.

■ AUTHOR INFORMATION

Corresponding Authors

Gabriel H. Ribeiro − *Departamento de Química, Universidade Federal de São Carlos, CEP 13565-905 São Carlos, São Paulo, Brazil;* orcid.org/0000-0003-0738-1638; Email: gabrielhenri10@hotmail.com

Alzir A. Batista − *Departamento de Química, Universidade Federal de São Carlos, CEP 13565-905 São Carlos, São Paulo, Brazil*; Phone: +55 1633518285; Email: daab@ufscar.br; Fax: +55 1633518350

Authors

Monize M. da Silva − *Departamento de Química, Universidade Federal de São Carlos, CEP 13565-905 São Carlos, São Paulo, Brazil*

Mariana S. de Camargo − *Departamento de Química, Universidade Federal de São Carlos, CEP 13565-905 São Carlos, São Paulo, Brazil*

Antônio G. Ferreira − *Departamento de Química, Universidade Federal de São Carlos, CEP 13565-905 São Carlos, São Paulo, Brazil*

Leandro Ribeiro − *Departamento de Química, Universidade Federal de São Carlos, CEP 13565-905 São Carlos, São Paulo, Brazil*

Marília I. F. Barbosa − *Departamento de Química, Universidade Federal de São Carlos, CEP 13565-905 São Carlos, São Paulo, Brazil*

Victor M. Deflon − *Instituto de Química de São Carlos, Universidade de São Paulo, CEP 13565-905 São Carlos, São Paulo, Brazil;* orcid.org/0000-0002-5368-6486

Silvia Castelli − *Dipartimento di Biologia, Università Tor Vergata di Roma, 00133 Rome, Italy*

Alessandro Desideri − *Dipartimento di Biologia, Università Tor Vergata di Roma, 00133 Rome, Italy*

Rodrigo S. Corrêa − *Departamento de Química, Universidade Federal de Ouro Preto, CEP 35400-000 Ouro Preto, Minas Gerais, Brazil*

Arthur B. Ribeiro − *Universidade de Franca, CEP 14404-600 Franca, São Paulo, Brazil;* orcid.org/0000-0002-4056-9571

Heloiza D. Nicolella − *Universidade de Franca, CEP 14404-600 Franca, São Paulo, Brazil*

Saulo D. Ozelin − *Universidade de Franca, CEP 14404-600 Franca, São Paulo, Brazil;* orcid.org/0000-0003-1769-4347

Denise C. Tavares − *Universidade de Franca, CEP 14404-600 Franca, São Paulo, Brazil;* orcid.org/0000-0003-4646-5914

Complete contact information is available at: https://pubs.acs.org/10.1021/acs.inorgchem.1c01539

Notes

The authors declare no competing financial interest.

■ ACKNOWLEDGMENTS

The authors are thankful for financial support from the following Brazilian Research Agencies: FAPESP (Processo 2018/19342-2), FAPEMIG, CNPq (Processo 422367/2018-4), and CAPES (this study was partially funded by Coordenação de Aperfeiçoamento de Pessoal de Nível Superior, Brasil (CAPES); Finance Code 001). R.S.C. is thankful for financial support by FAPEMIG (APQ-01674-18) and CNPq (Grants 403588/2016-2 and 308370/2017-1).

■ REFERENCES

(1) Allardyce, C. S.; Dyson, P. J. Metal-Based Drugs That Break the Rules. *Dalt. Trans.* **2016**, *45* (8), 3201−3209.

(2) Mari, C.; Pierroz, V.; Ferrari, S.; Gasser, G. Combination of Ru(II) Complexes and Light: New Frontiers in Cancer Therapy. *Chem. Sci.* **2015**, *6*, 2660−2686.

(3) Lin, K.; Zhao, Z.-Z.; Bo, H.-B.; Hao, X.-J.; Wang, J.-Q. Applications of Ruthenium Complex in Tumor Diagnosis and Therapy. *Front. Pharmacol.* **2018**, *9*, 1323−1333.

(4) Alessio, E.; Messori, L. NAMI-A and KP1019/1339, Two Iconic Ruthenium Anticancer Drug Candidates Face-to-Face: A Case Story in Medicinal Inorganic Chemistry. *Molecules* **2019**, *24* (10), 1995.

(5) Alessio, E. Thirty Years of the Drug Candidate NAMI-A and the Myths in the Field of Ruthenium Anticancer Compounds: A Personal Perspective. *Eur. J. Inorg. Chem.* **2017**, *2017* (12), 1549−1560.

(6) Nandi, P. G.; Jadi, P. K.; Das, K.; Prathapa, S. J.; Mandal, B. B.; Kumar, A. Synthesis of NNN Chiral Ruthenium Complexes and Their Cytotoxicity Studies. *Inorg. Chem.* **2021**, *60* (10), 7422−7432.

(7) Lovison, D.; Allegri, L.; Baldan, F.; Ballico, M.; Damante, G.; Jandl, C.; Baratta, W. Cationic Carboxylate and Thioacetate Ruthenium(Ii) Complexes: Synthesis and Cytotoxic Activity against Anaplastic Thyroid Cancer Cells. *Dalt. Trans.* **2020**, *49* (24), 8375−8388.

(8) Mitra, R.; Das, S.; Shinde, S. V.; Sinha, S.; Somasundaram, K.; Samuelson, A. G. Anticancer Activity of Hydrogen-Bond-Stabilized Half-Sandwich Ru II Complexes with Heterocycles. *Chem. - Eur. J.* **2012**, *18* (39), 12278−12291.

(9) de Sousa, I. H.; Campos, V. N. S.; Vale, A. A. M.; Maciel-Silva, V. L.; Leite, C. M.; Lopes, A. J. O.; Mourão, P. S.; das Chagas Alves Lima, F.; Batista, A. A.; de Azevedo dos Santos, A. P. S.; Almeida, M. A. P.; Pereira, S. R. F. Ruthenium (II) Complexes with N, O-

Chelating Proline and Threonine Ligands Cause Selective Cytotoxicity by the Induction of Genomic Instability, Cell Cycle Arrest and Apoptosis in Breast and Prostate Tumor Cells. *Toxicol. In Vitro* **2020**, *62*, 104679.
(10) Ribeiro, G. H.; Guedes, A. P. M.; de Oliveira, T. D.; de Correia, C. R. S. T. B.; Colina-Vegas, L.; Lima, M. A.; Nóbrega, J. A.; Cominetti, M. R.; Rocha, F. V.; Ferreira, A. G.; Castellano, E.; Teixeira, F.; Batista, A. A. Ruthenium(II) Phosphine/Mercapto Complexes: Their in Vitro Cytotoxicity Evaluation and Actions as Inhibitors of Topoisomerase and Proteasome Acting as Possible Triggers of Cell Death Induction. *Inorg. Chem.* **2020**, *59* (20), 15004.
(11) Kenny, R. G.; Marmion, C. J. Toward Multi-Targeted Platinum and Ruthenium Drugs - A New Paradigm in Cancer Drug Treatment Regimens? *Chem. Rev.* **2019**, *119* (2), 1058−1137.
(12) Trondl, R.; Heffeter, P.; Kowol, C. R.; Jakupec, M. A.; Berger, W.; Keppler, B. K. NKP-1339, the First Ruthenium-Based Anticancer Drug on the Edge to Clinical Application. *Chem. Sci.* **2014**, *5*, 2925−2932.
(13) Zeng, L.; Gupta, P.; Chen, Y.; Wang, E.; Ji, L.; Chao, H.; Chen, Z. S. The Development of Anticancer Ruthenium(II) Complexes: From Single Molecule Compounds to Nanomaterials. *Chem. Soc. Rev.* **2017**, *46* (19), 5771−5804.
(14) Thota, S.; Rodrigues, D. A.; Crans, D. C.; Barreiro, E. J. Ru(II) Compounds: Next-Generation Anticancer Metallotherapeutics? *J. Med. Chem.* **2018**, *61*, 5805−5821.
(15) Das, S.; Sinha, S.; Britto, R.; Somasundaram, K.; Samuelson, A. G. Cytotoxicity of Half Sandwich Ruthenium(II) Complexes with Strong Hydrogen Bond Acceptor Ligands and Their Mechanism of Action. *J. Inorg. Biochem.* **2010**, *104* (2), 93−104.
(16) Mukherjee, A.; Acharya, S.; Purkait, K.; Chakraborty, K.; Bhattacharjee, A.; Mukherjee, A. Effect of N, N Coordination and RuII Halide Bond in Enhancing Selective Toxicity of a Tyramine-Based RuII (p-Cymene) Complex. *Inorg. Chem.* **2020**, *59* (9), 6581−6594.
(17) Sudhindra, P.; Ajay Sharma, S.; Roy, N.; Moharana, P.; Paira, P. Recent Advances in Cytotoxicity, Cellular Uptake and Mechanism of Action of Ruthenium Metallodrugs: A Review. *Polyhedron*; Elsevier Ltd., December 1, 2020; DOI: 10.1016/j.poly.2020.114827.
(18) Mondelli, M. A.; Graminha, A. E.; Corrêa, R. S.; Da Silva, M. M.; Carnizello, A. P.; Von Poelhsitz, G.; Ellena, J.; Deflon, V. M.; Caramori, G. F.; Torre, M. H.; Tavares, D. C.; Batista, A. A. Ruthenium(II)/4,6-Dimethyl-2-Mercaptopyrimidine Complexes: Synthesis, Characterization, X-Ray Structures and in Vitro Cytotoxicity Activities on Cancer Cell Lines. *Polyhedron* **2014**, *68*, 312−318.
(19) Pires, W. C.; Lima, B. A. V.; de Castro Pereira, F.; Lima, A. P.; Mello-Andrade, F.; Silva, H. D.; da Silva, M. M.; Colina-Vegas, L.; Ellena, J.; Batista, A. A.; de Paul Silveira-Lacerda, E. Ru(II)/Diphenylphosphine/Pyridine-6-Thiolate Complexes Induce S-180 Cell Apoptosis through Intrinsic Mitochondrial Pathway Involving Inhibition of Bcl-2 and P53/Bax Activation. *Mol. Cell. Biochem.* **2018**, *438*, 199−217.
(20) Velozo-Sá, V. S.; Pereira, L. R.; Lima, A. P.; Mello-Andrade, F.; Rezende, M. R. M.; Goveia, R. M.; Pires, W. C.; Silva, M. M.; Oliveira, K. M.; Ferreira, A. G.; Ellena, J.; Deflon, V. M.; Grisolia, C. K.; Batista, A. A.; Silveira-Lacerda, E. P. In Vitro Cytotoxicity and in Vivo Zebrafish Toxicity Evaluation of Ru(II)/2-Mercaptopyrimidine Complexes. *Dalton Trans.* **2019**, *48*, 6026−6039.
(21) Da Silva, M. M.; De Camargo, M. S.; Correa, R. S.; Castelli, S.; De Grandis, R. A.; Takarada, J. E.; Varanda, E. A.; Castellano, E. E.; Deflon, V. M.; Cominetti, M. R.; Desideri, A.; Batista, A. A. Non-Mutagenic Ru(II) Complexes: Cytotoxicity, Topoisomerase IB Inhibition, DNA and HSA Binding. *Dalt. Trans.* **2019**, *48*, 14885−14897.
(22) Neves, S. P.; de Carvalho, N. C.; da Silva, M. M.; Rodrigues, A. C. B. C.; Bomfim, L. M.; Dias, R. B.; Sales, C. B. S.; Rocha, C. A. G.; Soares, M. B. P.; Batista, A. A.; Bezerra, D. P. Ruthenium Complexes Containing Heterocyclic Thioamidates Trigger Caspase-Mediated Apoptosis Through MAPK Signaling in Human Hepatocellular Carcinoma Cells. *Front. Oncol.* **2019**, *9*, 562−580.
(23) Corrêa, R. S.; Da Silva, M. M.; Graminha, A. E.; Meira, C. S.; Dos Santos, J. A. F.; Moreira, D. R. M.; Soares, M. B. P.; Von Poelhsitz, G.; Castellano, E. E.; Bloch, C.; Cominetti, M. R.; Batista, A. A. Ruthenium(II) Complexes of 1,3-Thiazolidine-2-Thione: Cytotoxicity against Tumor Cells and Anti-Trypanosoma Cruzi Activity Enhanced upon Combination with Benznidazole. *J. Inorg. Biochem.* **2016**, *156*, 153−163.
(24) Takarada, J. E.; Guedes, A. P. M.; Correa, R. S.; Silveira-Lacerda, E. de P.; Castelli, S.; Iacovelli, F.; Deflon, V. M.; Batista, A. A.; Desideri, A. Ru/Fe Bimetallic Complexes: Synthesis, Characterization, Cytotoxicity and Study of Their Interactions with DNA/HSA and Human Topoisomerase IB. *Arch. Biochem. Biophys.* **2017**, *636*, 28−41.
(25) Guedes, A. P. M.; Mello-Andrade, F.; Pires, W. C.; de Sousa, M. A. M.; da Silva, P. F. F.; de Camargo, M. S.; Gemeiner, H.; Amauri, M. A.; Gomes Cardoso, C.; de Melo Reis, P. R.; Silveira-Lacerda, E. P.; Batista, A. A. Heterobimetallic Ru(II)/Fe(II) Complexes as Potent Anticancer Agents against Breast Cancer Cells, Inducing Apoptosis through Multiple Targets. *Metallomics* **2020**, *12*, 547−561.
(26) da Silva, M.; de Camargo, M.; Castelli, S.; de Grandis, R.; Castellano, E.; Deflon, V.; Cominetti, M.; Desideri, A.; Batista, A. Ruthenium(II)-Mercapto Complexes with Anticancer Activity Interact with Topoisomerase IB. *J. Braz. Chem. Soc.* **2020**. DOI: 10.21577/0103-5053.20190214.
(27) Biancalana, L.; Pratesi, A.; Chiellini, F.; Zacchini, S.; Funaioli, T.; Gabbiani, C.; Marchetti, F. Ruthenium Arene Complexes with Triphenylphosphane Ligands: Cytotoxicity towards Pancreatic Cancer Cells, Interaction with Model Proteins, and Effect of Ethacrynic Acid Substitution. *New J. Chem.* **2017**, *41*, 14574−14588.
(28) Sáez, R.; Lorenzo, J.; Prieto, M. J.; Font-Bardia, M.; Calvet, T.; Omeñaca, N.; Vilaseca, M.; Moreno, V. Influence of PPh3Moiety in the Anticancer Activity of New Organometallic Ruthenium Complexes. *J. Inorg. Biochem.* **2014**, *136*, 1−12.
(29) de Camargo, M. S.; da Silva, M. M.; Correa, R. S.; Vieira, S. D.; Castelli, S.; D'Anessa, I.; De Grandis, R.; Varanda, E.; Deflon, V. M.; Desideri, A.; Batista, A. A. Inhibition of Human DNA Topoisomerase IB by Nonmutagenic Ruthenium(II)-Based Compounds with Antitumoral Activity. *Metallomics* **2016**, *8*, 179−192.
(30) Bjornsti, M. A.; Kaufmann, S. H. Topoisomerases and Cancer Chemotherapy: Recent Advances and Unanswered Questions. *F1000Research* **2019**, *8*, 1704.
(31) Pommier, Y. Diversity of DNA Topoisomerases 1I and Inhibitors. *Biochimie* **1998**, *80*, 255−270.
(32) You, F.; Gao, C. Topoisomerase Inhibitors and Targeted Delivery in Cancer Therapy. *Curr. Top. Med. Chem.* **2019**, *19* (9), 713−729.
(33) Gordon, E.; Ravicz, J.; Liu, S.; Chawla, S.; Hall, F. Cell Cycle Checkpoint Control: The Cyclin G1/Mdm2/P53 Axis Emerges as a Strategic Target for Broad-spectrum Cancer Gene Therapy - A Review of Molecular Mechanisms for Oncologists. *Mol. Clin. Oncol.* **2018**, *9*, 115−134.
(34) Tesauro, C.; Morozzo della Rocca, B.; Ottaviani, A.; Coletta, A.; Zuccaro, L.; Arnò, B.; Annessa, I. D.; Fiorani, P.; Desideri, A. Molecular Mechanism of the Camptothecin Resistance of Glu710Gly Topoisomerase IB Mutant Analyzed in Vitro and in Silico. *Mol. Cancer* **2013**, *12*, 100.
(35) Stewart, L.; Redinbo, M. R.; Qiu, X.; Hol, W. G. J.; Champoux, J. J. A Model for the Mechanism of Human Topoisomerase I. *Science (Washington, DC, U. S.)* **1998**, *279*, 1534−1541.
(36) Sordet, O.; Khan, Q. A.; Kohn, K. W.; Pommier, Y. Apoptosis Induced by Topoisomerase Inhibitors. *Curr. Med. Chem.: Anti-Cancer Agents* **2003**, *3*, 271−290.
(37) Pucci, B.; Kasten, M.; Giordano, A. Cell Cycle and Apoptosis 1. *Neoplasia* **2000**, *2*, 291−299.
(38) Appelt, P.; da Silva, J. P.; Fuganti, O.; Aquino, L. E. N.; Sandrino, B.; Wohnrath, K.; Santos, V. A. Q.; Cunha, M. A. A.; Veiga, A.; Murakami, F. S.; Back, D. F.; de Araujo, M. P. New Heterobimetallic Ruthenium (II) Complexes [Ru(N-S)(Bipy)-(Dppf)]PF6: Synthesis, Molecular Structure, Electrochemistry,

DFT, Antioxidant and Antibacterial Potential. *J. Organomet. Chem.* **2017**, *846*, 326−334.
(39) Qasim Warraich, M.; Ghion, A.; Perdisatt, L.; O'Neill, L.; Casey, A.; O'Connor, C. In Vitro Cytotoxicity, Cellular Uptake, Reactive Oxygen Species and Cell Cycle Arrest Studies of Novel Ruthenium(II) Polypyridyl Complexes towards A549 Lung Cancer Cell Line. *Drug Chem. Toxicol.* **2021**, *44*, 319.
(40) Sun, D.; Mou, Z.; Li, N.; Zhang, W.; Wang, Y.; Yang, E.; Wang, W. Anti-Tumor Activity and Mechanism of Apoptosis of A549 Induced by Ruthenium Complex. *JBIC, J. Biol. Inorg. Chem.* **2016**, *21*, 945−956.
(41) Nikolić, S.; Mihajlović-Lalić, L. E.; Vidosavljević, M.; Aranđelović, S.; Radulović, S.; Grgurić-Šipka, S. Mono- and Binuclear Ru(II) Arene Complexes with (Fluoro Substituted) Picolinic Acid: Synthesis, Characterization and Cytotoxicity. *J. Organomet. Chem.* **2019**, *902*, 120966.
(42) Obradović, D.; Nikolić, S.; Milenković, I.; Milenković, M.; Jovanović, P.; Savić, V.; Roller, A.; ĐorđićCrnogorac, M.; Stanojković, T.; Grgurić-Šipka, S. Synthesis, Characterization, Antimicrobial and Cytotoxic Activity of Novel Half-Sandwich Ru(II) Arene Complexes with Benzoylthiourea Derivatives. *J. Inorg. Biochem.* **2020**, *210*, 111164.
(43) Mohamed Subarkhan, M. K.; Ren, L.; Xie, B.; Chen, C.; Wang, Y.; Wang, H. Novel Tetranuclear Ruthenium(II) Arene Complexes Showing Potent Cytotoxic and Antimetastatic Activity as Well as Low Toxicity in Vivo. *Eur. J. Med. Chem.* **2019**, *179*, 246−256.
(44) Rahman, F. U.; Bhatti, M. Z.; Ali, A.; Duong, H. Q.; Zhang, Y.; Ji, X.; Lin, Y.; Wang, H.; Li, Z. T.; Zhang, D. W. Dimetallic Ru(II) Arene Complexes Appended on Bis-Salicylaldimine Induce Cancer Cell Death and Suppress Invasion via P53-Dependent Signaling. *Eur. J. Med. Chem.* **2018**, *157*, 1480−1490.
(45) Ribeiro, G. H.; Colina-Vegas, L.; Clavijo, J. C. T.; Ellena, J.; Cominetti, M. R.; Batista, A. A. Ru(II)/N-N/PPh_3 Complexes as Potential Anticancer Agents against MDA-MB-231 Cancer Cells (N-N = Diimine or Diamine). *J. Inorg. Biochem.* **2019**, *193*, 70.
(46) De Grandis, R. A.; Santos, P. W. da S. dos; Oliveira, K. M. de; Machado, A. R. T.; Aissa, A. F.; Batista, A. A.; Antunes, L. M. G.; Pavan, F. R. Novel Lawsone-Containing Ruthenium(II) Complexes: Synthesis, Characterization and Anticancer Activity on 2D and 3D Spheroid Models of Prostate Cancer Cells. *Bioorg. Chem.* **2019**, *85*, 455−468.
(47) Rilak Simović, A.; Masnikosa, R.; Bratsos, I.; Alessio, E. Chemistry and Reactivity of Ruthenium(II) Complexes: DNA/Protein Binding Mode and Anticancer Activity Are Related to the Complex Structure. *Coord. Chem. Rev.* **2019**, *398*, 113011−113037.
(48) Lee, P.; Wu, X. Review: Modifications of Human Serum Albumin and Their Binding Effect. *Curr. Pharm. Des.* **2015**, *21*, 1862−1865.
(49) Ghuman, J.; Zunszain, P. A.; Petitpas, I.; Bhattacharya, A. A.; Otagiri, M.; Curry, S. Structural Basis of the Drug-Binding Specificity of Human Serum Albumin. *J. Mol. Biol.* **2005**, *353* (1), 38−52.
(50) Rehman, S. U.; Sarwar, T.; Husain, M. A.; Ishqi, H. M.; Tabish, M. Studying Non-Covalent Drug-DNA Interactions. *Archives of Biochemistry and Biophysics*; Academic Press Inc., 2015; pp 49−60.
(51) Rohs, R.; Bloch, I.; Sklenar, H.; Shakked, Z.; Delbru, M. Molecular Flexibility in Ab Initio Drug Docking to DNA: Binding-Site and Binding-Mode Transitions in All-Atom Monte Carlo Simulations. *Nucleic Acids Res.* **2005**, *33*, 7048−7057.
(52) Staker, B. L.; Feese, M. D.; Cushman, M.; Pommier, Y.; Zembower, D.; Stewart, L.; Burgin, A. B. Structures of Three Classes of Anticancer Agents Bound to the Human Topoisomerase I - DNA Covalent Complex. *J. Med. Chem.* **2005**, *48*, 2336−2345.
(53) Santos, A. F.; Schiefer, E. M.; Atherino, M. C.; Atherino, J. C.; Negri, L. H.; Weffort-Santos, A. M.; Crisma, A. R.; de Souza, W. M.; Felipe, K. B. Schiefer Counter: An Alternative Method for Clonogenic Assay Evaluation. *J. Pharmacol. Toxicol. Methods* **2020**, *106*, 106911.
(54) Redinbo, M. R.; Champoux, J. J.; Hol, W. G. J. Novel Insights into Catalytic Mechanism from a Crystal Structure of Human Topoisomerase I in Complex with DNA †. *Biochemistry* **2000**, *39*, 6832−6840.
(55) Sheldrick, G. M. Crystal Structure Refinement with SHELXL. *Acta Crystallogr., Sect. C: Struct. Chem.* **2015**, *71*, 3−8.
(56) Macrae, C. F.; Sovago, I.; Cottrell, S. J.; Galek, P. T. A.; McCabe, P.; Pidcock, E.; Platings, M.; Shields, G. P.; Stevens, J. S.; Towler, M.; Wood, P. A. Computer Programs Mercury 4. 0: From Visualization to Analysis, Design and Prediction. *J. Appl. Crystallogr.* **2020**, *53*, 226−235.
(57) Sullivan, B. P.; Meyer, T. J. Comparisons of the Physical and Chemical Properties of Isomeric Pairs.' 2. Photochemical, Thermal, and Electrochemical Cis-Trans Isomerizations. *Inorg. Chem.* **1982**, *21*, 1037−1040.
(58) Baka, E.; Comer, J. E. A.; Takács-Novák, K. Study of Equilibrium Solubility Measurement by Saturation Shake-Flask Method Using Hydrochlorothiazide as Model Compound. *J. Pharm. Biomed. Anal.* **2008**, *46*, 335−341.
(59) Mosmann, T. Rapid Colorimetric Assay for Cellular Growth and Survival: Application to Proliferation and Cytotoxicity Assays. *J. Immunol. Methods* **1983**, *65*, 55−63.
(60) Gilroy, E. L.; Hicks, M. R.; Smith, D. J.; Rodger, A. Viscosity of Aqueous DNA Solutions Determined Using Dynamic Light Scattering. *Analyst* **2011**, *136* (20), 4159−4163.
(61) Naveenraj, S.; Anandan, S. Binding of Serum Albumins with Bioactive Substances − Nanoparticles to Drugs. *J. Photochem. Photobiol., C* **2013**, *14*, 53−71.
(62) Lakowicz, J. *Principles of Fluorescence Spectroscopy*; Springer, New York, 2006; Vol. *1*.
(63) Ross, P. D.; Subramanian, S. Thermodynamics of Protein Association Reactions: Forces Contributing to Stability1. *Biochemistry* **1981**, *20*, 3096−3102.
(64) Chillemi, G.; Fiorani, P.; Castelli, S.; Bruselles, A.; Benedetti, P.; Desideri, A. Effect on DNA Relaxation of the Single Thr718Ala Mutation in Human Topoisomerase I: A Functional and Molecular Dynamics Study. *Nucleic Acids Res.* **2005**, *33*, 3339−3350.
(65) Jones, G.; Willett, P.; Glen, R. C.; Leach, A. R.; Taylor, R. Development and Validation of a Genetic Algorithm for Flexible Docking. *J. Mol. Biol.* **1997**, *267*, 727−748.
(66) *Schrödinger Release 2021-2*; Maestro, Schrödinger: New York, 2021.
(67) BIOVIA, Dassault Systèmes. BIOVIA Pipeline Pilot. *BIOVIA Workbook*, Release 2020; Dassault Systèmes: San Diego, CA, 2020.
(68) Maron, D. M.; Ames, B. N. Revised Methods for the Salmonella Mutagenicity Test. *Mutat. Res.* **1983**, *113*, 173−215.
(69) Bernstein, L.; Kaldor, J.; Mccann, J.; Pike, M. C. An Empirical Approach to the Statistical Analysis of Mutagenesis Data from the Salmonella Test. *Mutat. Res.* **1982**, *97*, 267−281.
(70) Fenech, M. Cytokinesis-Block Micronucleus Cytome Assay. *Nat. Protoc.* **2007**, *2*, 1084−1104.
(71) Eastmond, D. A.; Tucker, J. D. Kinetochore Localization in Micronucleated Cytokinesis-Blocked Chinese Hamster Ovary Cells: A New and Rapid Assay for Identifying Aneuploidy-Inducing Agents. *Mutat. Res., Genet. Toxicol. Test.* **1989**, *224*, 517−525.
(72) Carnizello, A. P.; Barbosa, M. I. F.; Martins, M.; Ferreira, N. H.; Oliveira, P. F.; Magalhães, G. M.; Batista, A. A.; Tavares, D. C. In Vitro and in Vivo Antitumor Activity of a Novel Carbonyl Ruthenium Compound, the Ct-[RuCl(CO)(Dppb)(Bipy)]PF-6[Dppb = 1,4-Bis(Diphenylphosphine)Butane and Bipy = 2,2′-Bipyridine]. *J. Inorg. Biochem.* **2016**, *164*, 42−48.
(73) Qin, J.; Yuan, J.; Li, L.; Liu, H.; Qin, R.; Qin, W.; Chen, B.; Wang, H.; Wu, K. In Vitro and in Vivo Inhibitory Effect Evaluation of Cyclooxygenase-2 Inhibitors, Antisense Cyclooxygenase-2 CDNA, and Their Combination on the Growth of Human Bladder Cancer Cells. *Biomed. Pharmacother.* **2009**, *63*, 241−248.

https://doi.org/10.1021/acs.inorgchem.1c01539
Inorg. Chem. 2021, 60, 14174−14189